J. Fluid Mech. (2003), *vol.* 491, *pp.* 379–410.
DOI: 10.1017/S0022112003005664 Printed in the United Kingdom

Heat propagation from a concentrated external energy source in a gas

By V. KURDYUMOV[1], A. L. SÁNCHEZ[2] AND A. LIÑÁN[1]

[1]E. T. S. I. Aeronáuticos, Universidad Politécnica de Madrid,
Pl. Cardenal Cisneros 3, 28040 Madrid, Spain

[2]Departamento de Ingeniería Térmica y de Fluidos,
Universidad Carlos III de Madrid, 28911 Leganés, Spain

(Received 24 January 2003 and in revised form 14 May 2003)

This paper investigates the heat propagation process in a gas from concentrated energy sources with deposition times, t'_d, of the order of the characteristic acoustic time, t'_a, across the region where the temperature will be increased by a factor of order unity. Heat propagation takes place by two different mechanisms that act separately in two different neatly defined spatial regions of comparable size. Around the source, we find a conductive region of very high temperature where the spatial pressure variations are negligible. The edge of the resulting strongly heated low-density region appears as a contact surface that acts as a piston for the outer flow, where the pressure disturbances, of order of the ambient pressure in the distinguished regime $t'_d \sim t'_a$ considered here, generate a shock wave that heats up the outer gas as it propagates outwards. The mass and energy balances for the conductive region provide a differential equation linking its pressure with the velocity of its bounding contact surface, which is used, together with the jump conditions across the shock, when integrating the Euler equations for the outer compressible flow. Solutions for the heating history are obtained for point, line and planar sources for different values of the ratio t'_d/t'_a, including weak sources with $t'_d \gg t'_a$ and very intense sources with $t'_d \ll t'_a$. The solution determines in particular the temperature profile emerging as the pressure perturbations become negligible for times much larger than the acoustic time.

1. Introduction

The analysis of heat propagation from an energy source in a gas is of significance for many applications, including those related to combustion initiation. Depending on the rate of heat deposition, both pressure waves and thermal conduction can be responsible for heat propagation. If, for instance, the deposition time is sufficiently small, a problem reviewed in the article of Korobeinikov (1971), the resulting energy release is effectively instantaneous, leading to the formation of a strong shock wave that when propagating outwards is the main heating mechanism. Thermal conduction, on the other hand, is the dominant transfer mechanism when the deposition time is sufficiently large.

The present paper investigates the heating process in intermediate cases, due to a concentrated energy source in an infinite gas medium at rest with initial temperature, pressure and density T'_o, p'_o and ρ'_o. The analysis will be limited to symmetric plane, line and point sources, which are denoted with the subscript $j = (0, 1, 2)$; so that,

for instance, E_0, E_1 and E_2 represent, respectively, the energy per unit surface of the planar source, the energy per unit length of the line source, and the energy of the point source. This energy defines the characteristic size, r'_h, of the hot pocket where the temperature will eventually increase by a factor of order unity, according to

$$E_j = \frac{2^j \pi^{\delta_j}}{j+1} \rho'_o c_p T'_o r'^{j+1}_h, \tag{1.1}$$

where c_p is the specific heat at constant pressure, assumed for simplicity in the presentation to be constant, and $\delta_j = 0$ if $j = 0$ and $\delta_j = 1$ otherwise. The equal sign has been used in the above order-of-magnitude estimate to provide an accurate definition for r'_h, to be used as scale in the following development. The case of a concentrated source considered herein corresponds to external energy sources with a size r'_s much smaller than r'_h, for which the temperatures found around the source during the deposition period are much larger than the ambient value.

There exist two distinct characteristic times associated with r'_h, namely a time scale for conductive heat propagation across the hot pocket

$$t'_c = r'^2_h / \alpha_o, \tag{1.2}$$

with α_o representing the thermal diffusivity of the unperturbed gas, and an acoustic time scale for propagation of pressure disturbances

$$t'_a = r'_h / (p'_o/\rho'_o)^{1/2}, \tag{1.3}$$

where $(p'_o/\rho'_o)^{1/2}$ is, aside from a factor $\gamma^{1/2}$, the velocity of sound of the unperturbed gas, and γ denotes here the ratio of specific heats. The analysis refers to values of E_j leading to heated regions of size r'_h large compared with the ambient mean free path λ_o, of order $\alpha_o/(p'_o/\rho'_o)^{1/2}$, so that the continuum description of the flow applies. This implies that the ratio of the acoustic time to the conduction time,

$$\varepsilon = t'_a / t'_c \ll 1, \tag{1.4}$$

of the order of the Knudsen number of the reference state, λ_o/r'_h, is small compared with unity. We shall take ε as an asymptotically small parameter in the analysis.

The relative importance of heat conduction and mechanical pressure waves in the heat propagation process depends on the value of the deposition time, t'_d, during which the source remains active, to be compared with the characteristic times t'_c and t'_a. The pressure variations are small, and can be neglected, in the distinguished limit $t'_d \sim t'_c$, which was treated by Clarke, Kassoy & Riley (1984) for the plane source, and by Sánchez, Jiménez-Alvarez & Liñán (2003) for point and line sources. As the heat conduction from the source increases the temperature in a region of characteristic size r'_h by an amount of order T'_o, the resulting thermal expansion induces outwards velocities of order $r'_h/t'_d \ll (p'_o/\rho'_o)^{1/2}$; so that the flow is near-isobaric, and such that the heat transport by conduction and convection are comparable. The small pressure differences induced, of order $\varepsilon^2 p'_o$, can be neglected when writing the equation of state for the ideal gas. For the one-dimensional cases treated by Clarke *et al.* (1984) and by Sánchez *et al.* (2003) the momentum equation becomes secondary in the computation, in that the solution for the temperature and velocity fields can be obtained by integration of the continuity and energy equations, whereas the momentum equation can be used a posteriori to compute the small pressure differences that appear.

The other distinguished limit, which we address here, corresponds to energy sources with deposition times $t'_d \sim t'_a$, when the characteristic velocities induced during the

heating period are of the order of the unperturbed velocity of sound. As first noted by Clarke *et al.* (1984) in their analysis of the heating of a gas slot confined between two infinite parallel plates, both heat conduction and pressure waves play a role in this case, although the two mechanisms act separately in two neatly separated distinct regions, both of characteristic size r'_h, where the pressure rise relative to p'_o is of order unity. Around the source, there exists an inner conductive region of very hot gas, where, as we shall derive below from (2.5), the temperature is of order $T' \sim \varepsilon^{-1/(1+\sigma)} T'_o$, with σ, which typically ranges from $\sigma = 0.5$ to $\sigma = 0.75$ for non-ionized gases, representing the exponent for the assumed power-law temperature dependence of the thermal conductivity. The thermal expansion increases the pressure in this inner region and generates a convective flow proportial to the temperature gradient, with velocities, which in this regime $t'_d \sim t'_a$ are of order $(p'_o/\rho'_o)^{1/2}$, such that the convective and conductive transport of energy are of the same order. The resulting density in this region, $\rho' \sim \varepsilon^{1/(1+\sigma)} \rho'_o$, is very small, indicating that most of the gas that was originally in this hot region has been pushed out due to the overpressure. Due to the high temperatures found in this inner nearly hollow region the local Mach number is of order $\varepsilon^{1/[2(1+\sigma)]} \ll 1$, so that the spatial variations of the pressure are very small. Note that, despite the small densities found in the hot kernel, the local Knudsen number is still small, of order $\varepsilon^{1/[2(1+\sigma)]}$, so that the continuum description holds in this region.

The effect of heat conduction is confined to the inner hot region and to a thin transitional layer where $T' - T'_o$ is of order T'_o, so that heat effectively propagates only to a finite distance from the source. As a result, in the limit $\varepsilon \to 0$ the thermal wave has a sharp front, similar to that encountered by Zeldovich & Kompaneetz (1950) in the study of instantaneous heat deposition in a purely conductive medium with temperature-dependent conductivity and ambient temperature equal to zero. This thermal wave, which has been described for a constant heating rate by Clarke *et al.* (1984) in the planar case, and by Sánchez *et al.* (2003) in the cylindrical and spherical cases, appears to be bounded by a fluid surface that acts as a piston for the outer cold gas. The pressure waves produced by the rapid displacement of the outer fluid, with velocities of order $(p'_o/\rho'_o)^{1/2}$ in this limit $t'_d \sim t'_a$, generate a shock wave that propagates outwards, increasing the temperature by a factor of order unity in an outer region of characteristic size r'_h. The uniform pressure within the conductive region is that found at the piston-like contact surface, with a value that changes in time as dictated by the evolution of the outer compressible flow. The energy released at the source is employed to increase the internal energy of the inner conductive region and to mechanically displace the outer fluid. As we shall see below, the energy balance provides an equation for the motion of the contact surface in terms of the local pressure, to be used as boundary condition in integrating the Euler equations for the outer compressible flow. Note that the existence of an inner empty region was pointed out by Freeman (1968) and Dabora (1972) in their inviscid description of the self-similar blast waves induced by an energy source with a power-law dependence on time.

After the source has been turned off, the contact surface slows down, sending expansion waves that catch up with the leading shock wave, continuously weakening it. This weakening is additional to the one that for line and point sources is associated with geometrical effects. The process continues until the shock eventually becomes a weak wave of the acoustic type for times much larger than t'_a, as the pressure settles everywhere to the ambient value p'_o. In the hot pocket that remains, which conserves its two-region structure for times small compared with t'_c, the total energy released E_j

appears as an enthalpy increment according to

$$\int_0^\infty 2^j \pi^{\delta_j} \rho' c_p (T' - T'_o) r'^j \, \mathrm{d}r' = E_j, \tag{1.5}$$

where r' denotes the radial coordinate. Further evolution of the hot pocket, at times of the order t'_c, results from heat conduction and convection. In this final near-isobaric stage, the fluid displaced during the heating period flows back into the hollow conductive core as this cools down.

The application that motivates our interest in the problem is the initiation of a deflagration in a combustible mixture by an external energy source, as can be realized in practice by a spark, a laser beam or by passing an electric current through a thin wire. Recent efforts to compute numerically the phenomenon of spark ignition include the works of Kravchik & Sher (1994), Thiele, Warnatz & Maas (2000) and Thiele *et al.* (2002). The variable of interest is the minimum ignition energy, E_m, or critical value of E_j for which a self-sustained deflagration is formed following the deposition of heat. The success of the process depends on the competition between heat conduction, with a rate characterized by the conduction time across the hot pocket $t'_c = r'^2_h/\alpha_o$, and heat release by chemical reaction, which occurs with a characteristic time, δ_l^2/α_o, of the order of the residence time across the flame, δ_l/v_l, the ratio of the characteristic flame thickness $\delta_l = \alpha_o/v_l$ to the laminar flame propagation velocity v_l. When the energy deposition leads to a hot pocket such that its conduction time t'_c is smaller than the characteristic chemical time of the reactive mixture, the conductive heat loss to the ambient is too rapid to be compensated by the chemical heat release, and the deflagration initiation fails. As is well known, the critical value of E_m is associated with a value of t'_c of the order of the chemical time, which corresponds to a hot pocket of size r'_h of the order of the flame thickness δ_l.

The previous numerical simulations of Maas & Warnatz (1988) and Frendi & Sibulkin (1990) have shown that the external sources that give the smallest value of E_m for a given gas mixture are those with a size r'_s much smaller than $r'_h \sim \delta_l$ and a deposition time t'_d much smaller than $t'_c \sim \alpha_o/v_l^2$, a finding that motivates the present study of heating of a gas by a concentrated energy source, which we shall carry out in the distinguished limit $t'_d \sim t'_a$. Since the conduction time across the flame is of the order of the chemical time, the mixture remains chemically frozen during the heating period studied here. The temperature profile arising as the pressure settles to the ambient value for $t' \gg t'_a$ constitutes the appropriate initial condition for the numerical integration of the near-isobaric ignition process occurring for $t' \sim t'_c$. In that respect the process is significantly different from that of detonation initiation by energy sources. A detonation can form when the amount of energy released is such that r'_h is of the order of, although significantly larger than, the detonation thickness $\delta_d \sim (p'_o/\rho'_o)^{1/2}\delta_l/v_l \gg \delta_l$ (He & Clavin 1994). Since the characteristic reaction time $\delta_d/(p'_o/\rho'_o)^{1/2}$ is in this case comparable to the acoustic time t'_a, significant chemical reaction occurs during the deposition period. As a result, to study detonation initiation the frozen solutions described below need to be modified to account for chemical heat release, as done for planar sources by Clarke, Kassoy & Riley (1986) and Clarke *et al.* (1990).

Our interest in deflagration initiation problems leads us to generalize to point and line sources the work carried out by Clarke *et al.* (1984) for the planar case. In addition, since we are interested in the computation of the minimum ignition energy, we shall consider finite values of the deposition time t'_d and describe the flow structure

arising during both the heating period and post-heating period. For the investigation of Clarke *et al.* (1984), which refers only to the heating period, the energy flux q' (amount of energy deposited per unit time and per unit surface), rather than the energy deposited per unit surface E_0, is the relevant parameter characterizing the heating of the gas. The main parameter in their analysis is $\tilde{q}_w$, which, aside from an irrelevant factor of order unity, corresponds to the dimensionless heating rate $q'/[p'_o(p'_o/\rho'_o)^{1/2}]$. They considered the near-isobaric case, corresponding to small heating rates $q'/[p'_o(p'_o/\rho'_o)^{1/2}] \ll 1$ such that the characteristic velocity induced by thermal expansion, which is of order q'/p'_o, is much smaller than the velocity of sound, of order $(p'_o/\rho'_o)^{1/2}$. The case of strong heating, $q'/[p'_o(p'_o/\rho'_o)^{1/2}] \sim O(1)$, was also considered, noting in particular that during the early stages of the heating process, when the amount of heat released is such that the temperature at the source has increased only by a factor of order unity, the size of the hot pocket, of order $\alpha_o p'_o/q'$, is comparable to the ambient mean free path, λ_o, so that the continuum description of the flow does not apply at these early times of the order of the ambient molecular collision time, t'_λ. However, the Navier–Stokes equations apply for larger times, when the two-region structure discussed above, which includes an inner conductive kernel of very high temperature and an outer inviscid region bounded externally by a shock wave, has already developed. The same two-region structure is encountered in our work, which considers only situations in which the heat is released at times $t'_d \sim t'_a$ much larger by a factor ε^{-1} than t'_λ, and the size of the heated region r'_h is also larger than λ_o by the same factor. Under these conditions, the validity of the continuum description is guaranteed, this being the case in deflagration initiation applications.

The paper is structured as follows. First, we shall give in § 2 the non-dimensional formulation of the problem, using the scales corresponding to the case $\varepsilon \ll 1$ with $t'_d \sim t'_a$. The simplified formulation for the limit $\varepsilon \to 0$ is given next in § 3. The following two sections are devoted to the limiting cases of instantaneous heat deposition ($t'_d \ll t'_a$) and near-isobaric heat deposition ($t'_a \ll t'_d \ll t'_c$). Energy sources with $t'_d \sim t'_a$ will be investigated in § 6, with particular attention given to the case of a constant heating rate. The evolution of the flow after the source has been turned off will be considered next, and the asymptotic temperature and energy distributions emerging for $t' \gg t'_a$ will be determined for different values of t'_d/t'_a. Concluding remarks will be offered in the final section.

2. Formulation

The scales identified above for the heating period can be used to define a dimensionless coordinate $r = r'/r'_h$, a dimensionless time $t = t'/t'_a$, and a dimensionless velocity $v = v'/(p'_o/\rho'_o)^{1/2}$. With this selection for the time scale, the dimensionless deposition time

$$t_d = t'_d/t'_a, \tag{2.1}$$

of order unity in the distinguished limit considered here, becomes the appropriate parameter to characterize the intensity of the energy source. Temperature, density and pressure are scaled with their initial values to give $T = T'/T'_o$, $\rho = \rho'/\rho'_o$ and $p = p'/p'_o$. Use of these variables enables the problem to be written in an appropriate dimensionless form that serves to illustrate the character of the solution when $t'_d \sim t'_a$. For instance, for the line source the corresponding non-dimensional conservation

equations become

$$\frac{\partial \rho}{\partial t}+\frac{1}{r}\frac{\partial}{\partial r}(r\rho v)=0, \tag{2.2}$$

$$\rho\left(\frac{\partial v}{\partial t}+v\frac{\partial v}{\partial r}\right)+\frac{\partial p}{\partial r}=Pr\ \varepsilon\left\{\frac{\partial}{\partial r}\left[T^{\sigma}\left(\frac{4}{3}\frac{\partial v}{\partial r}-\frac{2}{3}\frac{v}{r}\right)\right]+\frac{2T^{\sigma}}{r}\left(\frac{\partial v}{\partial r}-\frac{v}{r}\right)\right\}, \tag{2.3}$$

$$\frac{1}{\gamma}\frac{\partial p}{\partial t}+\frac{1}{r}\frac{\partial}{\partial r}(rvp)-\frac{\gamma-1}{\gamma}v\frac{\partial p}{\partial r}=\frac{\varepsilon}{r}\frac{\partial}{\partial r}\left(rT^{\sigma}\frac{\partial T}{\partial r}\right)$$
$$+2Pr\ \varepsilon\frac{\gamma-1}{\gamma}\left[\left(\frac{\partial v}{\partial r}\right)^{2}+\left(\frac{v}{r}\right)^{2}-\frac{1}{3r^{2}}\left(\frac{\partial rv}{\partial r}\right)^{2}\right]. \tag{2.4}$$

These equations, supplemented with the equation of state for the ideal gas $p=\rho T$, must be integrated with the initial and boundary conditions

$$\begin{aligned} &t=0: \quad \rho=p=1, \qquad v=0,\\ &t>0: \quad \left\{\begin{array}{ll} r\to 0: & v=0, \quad 2r\varepsilon T^{\sigma}\partial T/\partial r=-q/t_d,\\ r=\infty: & \rho=p=T=1, \quad v=0. \end{array}\right\} \end{aligned} \tag{2.5}$$

The analysis assumes a power law $k/k_o=\mu/\mu_o=(T'/T'_o)^{\sigma}$ for the variation with temperature of the thermal conductivity k and viscosity μ from their unperturbed values k_o and μ_o. A value $\sigma=0.5$ is used in this paper for the exponent in the power law, which corresponds approximately to non-ionized gases at high temperature. The dependence of k on temperature is considerably stronger in electronic conduction in plamas, for which $\sigma=2.5$. We shall see below that in the limit $\varepsilon\to 0$ considered here the solution becomes independent of the Prandtl number of the gas mixture, $Pr=\mu c_p/k$, which appears however as a parameter in the complete equations given above.

The heating rate from the source q' is non-dimensionalized with its characteristic value E_j/t'_d to give the heating function $q(t)=q'/(E_j/t'_d)$, of order unity, which must satisfy $\int_0^{t_d} q\,\mathrm{d}t=t_d$ and vanishes for $t\geqslant t_d$. Note that this definition yields $q=1$ for the source of constant rate. An example of the results of integrations of the above problem is shown in figure 1 for $q=1$, $t_d=1$ and $\varepsilon=0.001$. The inner thermal wave of uniform pressure and the outer compressible flow preceded by a leading shock wave are clearly visible in the plot. To expose more clearly the two-region structure that emerges, the profiles of temperature and pressure corresponding to the instant $t=0.8$ have been plotted separately in figure 2, where the associated instantaneous location of the contact surface, r_e, and of the shock wave, r_s, are indicated with a dashed line.

3. Asymptotic analysis for $\varepsilon\ll 1$

The equations for the description of these two regions, which are also given below for the plane and point source by incorporating the index j in the formulation, follow naturally from the above problem by considering the limit $\varepsilon\ll 1$. Thus, the boundary condition for the heat flux at the source given in (2.5) indicates that the temperature increases around the source to a large value of order $\varepsilon^{-1/(\sigma+1)}$, which is used to define a rescaled temperature $\theta=\varepsilon^{1/(\sigma+1)}T$ of order unity in the inner hot region. On the other hand, an order-of-magnitude balance between the pressure gradient and the gas acceleration in the momentum equation (2.3) yields a small value of order $\varepsilon^{1/(\sigma+1)}$ for the spatial pressure variations in this inner hot region, where r and v are of order unity. Then, when writing the conservation equations for mass and energy we can

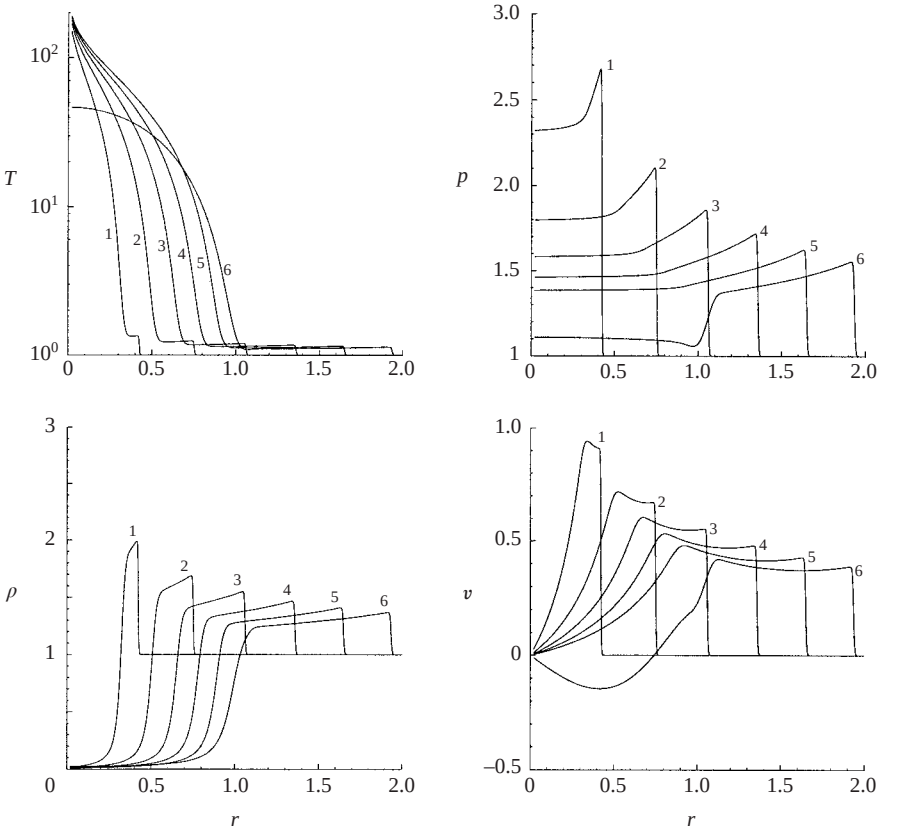

FIGURE 1. Profiles of temperature, pressure, density and velocity at $t = 0.2$ (1), $t = 0.4$ (2), $t = 0.6$ (3), $t = 0.8$ (4), $t = 1.0$ (5), and $t = 1.2$ (6) obtained for $q = 1$, $\varepsilon = 0.001$ and $t_d = 1$ from integration of (2.2)–(2.5).

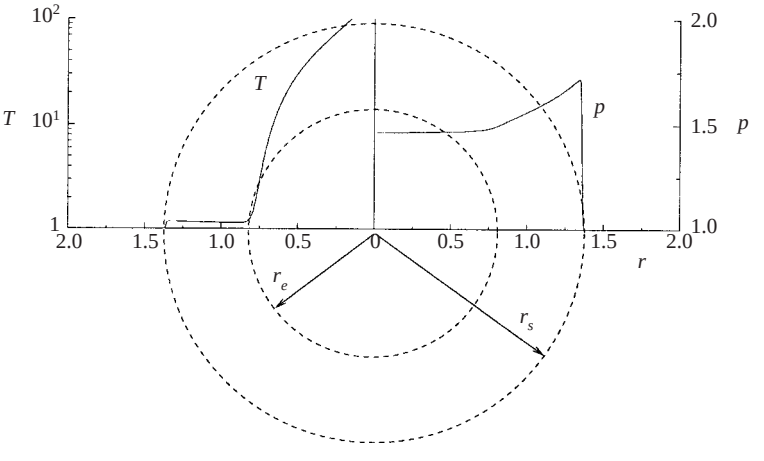

FIGURE 2. Profiles of temperature and pressure at $t = 0.8$ obtained for $q = 1$, $\varepsilon = 0.001$ and $t_d = 1$ from integration of (2.2)–(2.5).

consider the pressure to be $p_e(t)$, uniform in the hot gas, equal to that found at the edge of the thermal wave, so that (2.2) and (2.4) simplify to

$$\frac{\partial}{\partial t}\left(\frac{p_e}{\theta}\right)+\frac{1}{r^j}\frac{\partial}{\partial r}\left(\frac{r^j p_e v}{\theta}\right)=0 \tag{3.1}$$

and

$$\frac{1}{\gamma}\frac{\mathrm{d}p_e}{\mathrm{d}t}+\frac{1}{r^j}\frac{\partial}{\partial r}\left[r^j\left(p_e v-\theta^\sigma\frac{\partial\theta}{\partial r}\right)\right]=0. \tag{3.2}$$

In writing (3.2) we have also left out the viscous dissipation terms in (2.4), which are of order ε. As in (2.5), the boundary conditions at the origin $r=0$ are $v=0$ and $(j+1)r^j\theta^\sigma\partial\theta/\partial r=-q/t_d$.

Using the boundary conditions at $r=0$ in a first quadrature of (3.2) gives

$$\frac{r^{j+1}}{\gamma}\frac{\mathrm{d}p_e}{\mathrm{d}t}+(j+1)r^j\left(p_e v-\theta^\sigma\frac{\partial\theta}{\partial r}\right)=q/t_d, \tag{3.3}$$

which determines v in terms of the temperature distribution and $p_e(t)$. According to (3.3) the external heat is locally accumulated in the hot region or transported by convection or conduction. In the distinguished regime $t_d\sim O(1)$, the three terms on the left-hand side of (3.3) are of the same order, while for $t_d\gg 1$ the pressure $p_e\simeq 1$ remains constant, and convection and conduction cooperate to transport the heat away from the deposition region.

Substituting (3.3) into (3.1) provides the equation

$$\frac{\partial}{\partial t}\left(\frac{p_e}{\theta}\right)+\frac{1}{r^j}\frac{\partial}{\partial r}\left[\frac{1}{\theta}\left(\frac{q}{(j+1)t_d}-\frac{r^{j+1}}{(j+1)\gamma}\frac{\mathrm{d}p_e}{\mathrm{d}t}+r^j\theta^\sigma\frac{\partial\theta}{\partial r}\right)\right]=0 \tag{3.4}$$

to be integrated with initial and boundary conditions

$$\begin{aligned} &t=0: \quad \theta=0,\\ &t>0: \quad \left\{\begin{array}{ll} r\to 0: & (j+1)r^j\theta^\sigma\,\partial\theta/\partial r=-q/t_d,\\ r=r_e: & \theta=0 \quad\text{and}\quad \theta^\sigma\partial\theta/\partial r=0,\end{array}\right\}\end{aligned} \tag{3.5}$$

where we have included the additional conditions at the edge, $r=r_e(t)$, of the hot region heated by conduction, outside which θ is of order $\varepsilon^{1/(\sigma+1)}$, negligible in the first approximation. The above problem is coupled to the outer inviscid compressible flow problem, which must be solved to determine the location of the thermal-wave edge $r_e(t)$ as well as the value for the pressure there $p_e(t)$.

Since ρ, of order $\varepsilon^{1/(\sigma+1)}$, is negligible in the first approximation at $r<r_e$ in the limit $\varepsilon\to 0$, the edge of the thermal wave behaves as a contact surface, so that

$$v=\frac{\mathrm{d}r_e}{\mathrm{d}t}=\dot{r}_e. \tag{3.6}$$

Using this equation in evaluating (3.3) at $r=r_e$, together with the condition that the heat flux vanish there, provides the energy balance

$$\frac{r_e^{j+1}}{\gamma}\frac{\mathrm{d}p_e}{\mathrm{d}t}+p_e\frac{\mathrm{d}r_e^{j+1}}{\mathrm{d}t}=\frac{q}{t_d}, \tag{3.7}$$

which states that the heat added is partly employed to increase the internal energy of the hot conductive pocket and partly employed to displace the outer cold fluid.

To anticipate the form of $\theta(r,t)$ near the edge $r=r_e$ of the thermal wave, it is convenient to write (3.4) in terms of the local coordinate $x=(r_e-r)/\delta$, which uses a

time-dependent thickness $\delta(t)$, as done by Carrier, Fendell & Marble (1975) for the analysis of unsteady mixing layers with time-dependent strain rate. Assuming a local description for small x of the form $\theta = x^{\beta}$, and with terms of higher order in x being neglected, yields, after subtraction of (3.7),

$$p_e \delta \delta_t + \left[\frac{jq}{(j+1) t_d r_e^{j+1}} + \frac{1}{\gamma} \left(\frac{1}{j+1} + \frac{\gamma - 1}{\beta} \right) \frac{\mathrm{d}p_e}{\mathrm{d}t} \right] \delta^2 = (1 - \sigma\beta) x^{(\sigma+1)\beta - 2}. \tag{3.8}$$

The selection $\beta = 2/(\sigma+1)$ gives a balance among all of the terms above, reducing (3.8) to an ordinary differential equation for the evolution of δ, which can be integrated to give

$$\delta^2 = \frac{2(1-\sigma)}{1+\sigma} \int_0^t \exp\left\{ - \int_{t^*}^t \left[\frac{2jq}{(j+1) t_d r_e^{j+1}} + \left(\frac{1}{j+1} + \frac{\gamma - 1}{2/(\sigma+1)} \right) \frac{2}{\gamma} \frac{\mathrm{d}p_e}{\mathrm{d}t} \right] \frac{\mathrm{d}t^{**}}{\mathrm{p}_e} \right\} \frac{\mathrm{d}t^*}{p_e} \tag{3.9}$$

where the integration constant has been selected to give a bounded value for δ at $t = 0$ and where t^* and t^{**} are appropriate intermediate dummy variables for integration. The asymptotic behaviour $\theta = x^{2/(\sigma+1)}$ of the temperature profile at $r_e - r \ll 1$ yields $\theta^{\sigma} \theta_x = 2x/(\sigma+1)$, indicating that the conduction flux decreases linearly as the contact surface is approached. Note that, as can be inferred from the multiplying factor in (3.9), the local asymptotic description $\theta = [(r_e - r)/\delta]^{2/(\sigma+1)}$ is only valid for $\sigma < 1$. When the temperature dependence of the thermal conductivity is stronger, the temperature is seen to approach its boundary with an infinite gradient, in a local balance between heat conduction and convection induced by the temperature gradient. The corresponding exponent $\beta = 1/\sigma$ of the resulting local solution $\theta = x^{1/\sigma}$ is determined by equating to zero the right-hand side of (3.8), while the computation of $\delta(t)$ requires in this case numerical integration of (3.4) and (3.5). Correspondingly, the conduction flux is seen to decay more slowly as the bounding contact surface is approached, as can be seen from $\theta^{\sigma} \theta_x = x^{1/\sigma}/\sigma$. Also of interest is that the asymptotic behaviour for the intermediate case $\sigma = 1$ is of the form $\theta = x(\ln x^{-1})^{1/2}$ with $\theta^{\sigma} \theta_x \simeq x(\ln x^{-1})$, a result due to Clarke *et al.* (1984).

In the outer region, $r > r_e$, where r is also of order unity, the values of v, p, ρ and T are of order unity. The characteristic Reynolds number is of order $\varepsilon^{-1} \gg 1$, and molecular diffusion can be neglected in the first approximation when describing the outer motion. The resulting Euler equations are given by (2.2)–(2.4) for $j = 1$ without the terms on their right-hand sides, which are of order ε. They must be integrated with the boundary conditions at $r = r_e(t)$ given above in (3.6) and (3.7). The external heating rate in general gives rise to the formation of a shock wave, at $r = r_s$, that propagates into the cold unperturbed gas. The density, ρ_s, velocity, v_s, and pressure, p_s, behind the shock, and the shock velocity, $\dot{r}_s$, are related though the jump conditions (Landau & Lifshitz 1987)

$$\left.\begin{aligned} \dot{r}_s = \frac{\mathrm{d}r_s}{\mathrm{d}t} &= \left(\frac{(\gamma-1) + (\gamma+1) p_s}{2} \right)^{1/2}, \\ \dot{r}_s - v_s &= \left(\frac{[(\gamma+1) + (\gamma-1) p_s]^2}{2[(\gamma-1) + (\gamma+1) p_s]} \right)^{1/2}, \\ \rho_s &= \frac{(\gamma-1) + (\gamma+1) p_s}{(\gamma+1) + (\gamma-1) p_s}, \end{aligned}\right\} \tag{3.10}$$

where $r_s(t)$ is the location of the shock.

Integration of the Euler equations with boundary conditions (3.6) and (3.7) at $r = r_e$ and (3.10) at $r = r_s$ determines for a given heating rate $q(t)$ the dynamics of the outer compressible flow, which turns out to be independent of the value of σ, and clearly will be valid for any $k(T)$. The solution includes the instantaneous location of the contact surface $r_e(t)$ and that of the leading shock wave $r_s(t)$, along with the evolution of the hot-kernel pressure $p_e(t)$, needed to integrate the problem (3.4) and (3.5) for the structure of the conductive thermal wave corresponding to $0 < r < r_e$. Note that once the source is shut off for $t > t_d$, the energy balance (3.7) for the contact surface reduces to

$$\frac{\mathrm{d}}{\mathrm{d}t}\left(p_e r_e^{(j+1)\gamma}\right) = 0, \tag{3.11}$$

indicating that the evolution of the inner hot region is globally isentropic in the post-heating period.

4. Instantaneous heat deposition

The formulation given above corresponds to the leading-order description in the asymptotic analysis for $\varepsilon \ll 1$ of the heating process from a small source in the distinguished limit $t_d \sim 1$. Consideration of extreme values of t_d serves to analyse limiting cases of interest. Thus, the limit $t_d \ll 1$ corresponds to instantaneous heat deposition. A straightforward order-of-magnitude analysis of (3.10) indicates that the shock wave becomes very strong in this limit; it propagates with a velocity of order $\dot{r}_s \sim t_d^{-(j+1)/(j+3)}$, elevating the pressure of the gas to a large value of order $t_d^{-2(j+1)/(j+3)} p_o'$. Since the contact surface also moves with a velocity of order $\dot{r}_e \sim t_d^{-(j+1)/(j+3)}$, as indicated by (3.7), both the contact surface and the shock wave are located at a small radius of order $r_e \sim r_s \sim t_d^{2/(j+3)}$ when the energy release ends at $t = t_d$. The strong shock keeps propagating outwards as it weakens, reaching distances of order r_h' at times of order t_a', that is, $r_s \sim O(1)$ for $t \sim O(1)$. The contact surface bounding the conductive region also moves outwards as the pressure decreases, as can be seen by using (3.11), but only to occupy a final asymptotic location $r_a \sim t_d^{2(\gamma-1)/[\gamma(j+3)]} \ll 1$, when $p_e \to 1$ for $t \gg 1$. Therefore, although a hot conductive region always exists in the inmediate vicinity of the energy source, its size becomes very small, compared with r_h', in the limit $t_d \ll 1$ of very intense sources. Correspondingly, the radius of this conductive core can be neglected in the first approximation for the description of the blast wave that arises following the deposition of heat when $t_d \ll 1$.

The solution requires numerical integration of the Euler equations with the boundary conditions (3.10) at the leading shock wave. If one forces the velocity at the origin to vanish and the solution to satisfy the energy conservation balance

$$\frac{\gamma}{\gamma - 1} = (j+1)\int_0^{r_s}\left[\frac{p-1}{\gamma-1} + \frac{1}{2}\rho v^2\right] r^j \,\mathrm{d}r, \tag{4.1}$$

then the conditions (3.7) and (3.10) are automatically satisfied for $t > t_d$. The numerical solution, which was first obtained by Goldstine & Neumann (1955) and Brode (1955) for the spherical blast and by Korobeinikov & Chushkin (1966) for the cylindrical and planar blasts, determines in particular the evolution of the leading shock wave from the self-similar blast wave of Sedov (1946) and Taylor (1950), for $t \ll 1$, to a very weak shock moving with a velocity slightly larger than the velocity of sound for $t \gg 1$. In this latter limit, the shock is located at a large distance $r_s \gg 1$ from the source,

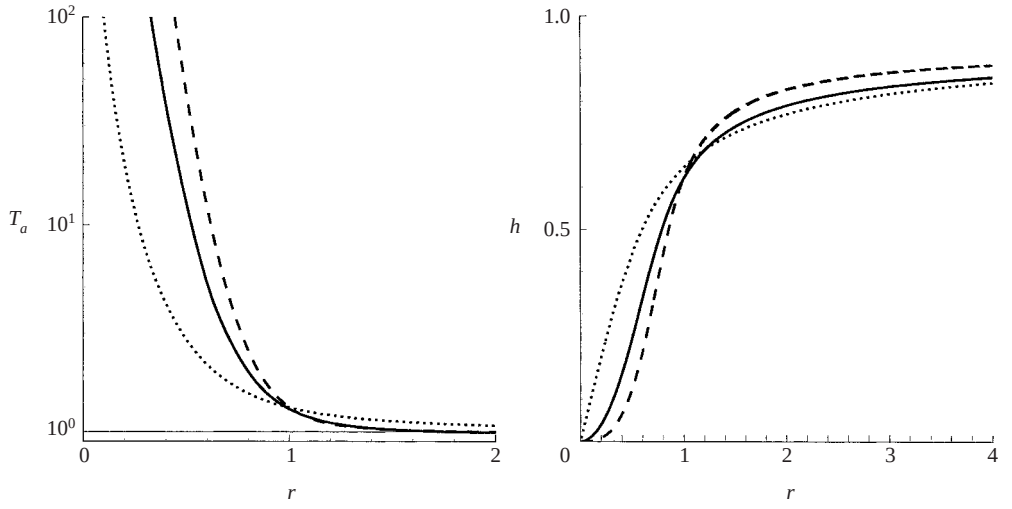

FIGURE 3. The profiles of T_a and h corresponding to instantaneous heat deposition from a planar source (dotted line), a line source (solid line), and a point source (dashed line).

leaving a growing central region of stagnant gas where the pressure has recovered the atmospheric value. The structure of the resulting near-acoustic wave shows a region of overpressure and positive velocity inmediately behind the weak leading shock followed by a trailing region of reverse flow where the pressure is smaller than p'_o. Landau (1945) was the first to describe the asymptotic decay laws for cylindrical and spherical waves, whose strengths decrease according to $p-1\sim v\sim r_s^{-3/4}$ and $p-1\sim v\sim r_s^{-1}(\ln r_s)^{-1/2}$, respectively, while the strength of the planar wave decays somewhat faster ($p-1\sim v\sim r_s^{-1/2}$). Because of the existence of the intermediate rarefaction region, a second shock wave must appear eventually as explained by Landau (1945) and Whitham (1950), thereby yielding an N-wave for the final structure of the near-acoustic wave. This transition to Landau's N-wave solution is postponed to a very late stage of the flow evolution however. This was numerically ascertained by Okhotsimskii & Vlasova (1962), who extended their numerical integrations well beyond the ranges previously explored by Goldstine & Neumann (1955) and Brode (1955). Their computations indicate that a second shock indeed emerges, but only for rescaled times $t\gtrsim 5000$, when $p_s\lesssim 5\times 10^{-5}$.

As a result of the shock heating, the isobaric stagnant solution encountered for $t\gg 1$ exhibits a characteristic temperature distribution, $T_a(r)$, which constitutes the initial condition for studies of deflagration initiation from intense energy sources with $t_d\ll 1$. According to Okhotsimskii & Vlasova (1962), the second shock wave only appears as a negligibly weak discontinuity for extremely large times, so that its effect on the asymptotic temperature distribution can be neglected. The condition that each fluid particle conserves its entropy after crossing the leading shock enables the computation of $T_a(r)$ for a given leading-shock history. The solution can be written in parametric form in terms of the values of the pressure and density of the shocked gas, $p_s(r_s)$ and $\rho_s(r_s)$, corresponding to a shock location r_s. The final temperature of the shocked particle after expanding isentropically to the ambient pressure becomes $T_a=p_s^{1/\gamma}/\rho_s$, while its final location is given by integrating the continuity equation to give $r^{j+1}=(j+1)\int_0^{r_s}[p_s(\xi)^{1/\gamma}/\rho_s(\xi)]\xi^j\,\mathrm{d}\xi$. The distributions of $T_a(r)$ are shown in figure 3

for $\gamma = 1.4$, along with the fraction of energy stored up to the radius r

$$h = \frac{\int_0^{r'} 2^j \pi^{\delta_j} \rho' c_p (T' - T'_o) r'^j \, \mathrm{d}r}{E_j} = (j+1) \int_0^r \left(1 - \frac{1}{T_a}\right) r^j \, \mathrm{d}r. \tag{4.2}$$

As can be seen in figure 3, this fraction approaches only slowly its limiting value $h = 1$ for $r \gg 1$, in agreement with the asymptotic analysis of Landau (1945), who predicted that the energy of the near-acoustic wave decays according to $1 - h \sim r_s^{-1/2}$ for $j = 0$, $1 - h \sim r_s^{-1/4}$ for $j = 1$ and $1 - h \sim (\ln r_s)^{-1/2}$ for $j = 2$. Moreover, the comparison between the plots of $T_a(r)$ and $h(r)$ reveals that a significant fraction of the energy is employed to generate a small change in the temperature of the gas located far from the source. Implications of this finding for the problem of deflagration initiation are to be discussed later.

5. Near-isobaric heating

In the opposite limit $t_d \gg 1$, equations (3.4)–(3.10) also describe the heating of a gas from a source with a deposition time much larger than the acoustic time t'_a, and yet much smaller than t'_c, so that the two-region asymptotic structure still holds. Since the contact surface moves with a velocity of order r'_h/t'_d, the characteristic Mach number for the motion induced for $r > r_e$ is $t_d^{-1} \ll 1$, while the characteristic Reynolds number, of order t'_c/t'_d, remains large provided $t'_d \ll t'_c$. The resulting outer inviscid motion is in first approximation that of an incompressible fluid at $r'/r'_e \sim 1$, with small departures at $r' \sim (p_o/\rho_o)^{1/2} t'$, which can be computed from the acoustic equations by considering the linearized form of (3.6), (3.7) and (3.10) around $p_e = 1$, as done by Clarke *et al.* (1984) for planar sources and by Deshaies & Clavin (1979) for spherical sources. In this near-isobaric limit $p_e \simeq 1$, and equation (3.7) can be integrated to give $r_e^{j+1} = \int_0^t (q/t_d)\, \mathrm{d}t$, thereby enabling the computation of the thermal wave existing for $0 < r < r_e$ independently of the outer acoustic flow.

5.1. *The reduced problem*

For the analysis of the heat sources in the intermediate range $t'_a \ll t'_d \ll t'_c$, it is convenient to measure the time with t'_d and the gas velocity with $r'_h/t'_d \ll (p'_o/\rho'_o)^{1/2}$ by introducing the alternative variables of order unity $\tau = t/t_d$ and $u = t_d v$, while $\Theta = t_d^{1/(\sigma+1)} \theta$ becomes the appropriate temperature variable, which is of order unity, as can be anticipated from the heat flux condition (3.5). Since the pressure increments $p_e - 1$ in the conductive core are of order t_d^{-1}, the accumulation of internal energy can be neglected in the first approximation in the energy balance (3.7), which can be integrated to yield the location of the contact surface

$$r_e = \left(\int_0^\tau q \, \mathrm{d}\tau \right)^{1/(j+1)}, \tag{5.1}$$

where the heating function $q(\tau)$ must satisfy $\int_0^1 q \, \mathrm{d}\tau = 1$ and $q = 0$ for $\tau > 1$. The resulting near-isobaric thermal wave can be solved in the first approximation, independently of the outer inviscid field, by integrating the heat equation

$$\frac{1}{\Theta^2} \frac{\partial \Theta}{\partial \tau} - \frac{1}{r^j} \frac{\partial}{\partial r} \left[\frac{1}{\Theta} \left(\frac{q}{(j+1)} + r^j \Theta^\sigma \frac{\partial \Theta}{\partial r} \right) \right] = 0, \tag{5.2}$$

with the initial and boundary conditions

$$\tau = 0: \quad \Theta = 0,$$
$$\tau > 0: \quad \begin{cases} r \to 0: & (j+1) r^j \Theta^\sigma \partial\Theta/\partial r = -q, \\ r = r_e: & \Theta = 0, \quad \Theta^\sigma \partial\Theta/\partial r = 0. \end{cases} \tag{5.3}$$

The solution is seen to depend on the thermal-conductivity exponent σ and on the heating rate $q(\tau)$, which is applied during a finite period $0 < \tau \leqslant 1$. According to the flux condition at $r = 0$, the temperature remains bounded at the source for $j = 0$, but grows to infinity at $r = 0$ for the line and point source, for which

$$\Theta^{\sigma+1} \sim -(\sigma+1)(q/2) \ln r \quad \text{and} \quad \Theta^{\sigma+1} \sim (\sigma+1)/(3r), \tag{5.4}$$

respectively, as $r \to 0$. For a realistic source of finite size, the temperature profile flattens as the source is approached, reaching a peak value at $r = 0$ that depends on the source size. With convection being negligible in this near-source region, the solution is determined by a balance of conduction and external heating, giving a temperature profile, not computed here, that matches with the asymptotic solutions given in (5.4).

During the period of heat deposition, the thermal expansion sets the gas in motion away from the source, yielding a thermal wave with an increasing radius given in (5.1). The velocity field

$$u = \frac{1}{r^j} \left(\frac{q}{j+1} + r^j \Theta^\sigma \frac{\partial \Theta}{\partial r} \right) \tag{5.5}$$

obtained from (3.3) in this near-isobaric limit reduces to $u = q/[(j+1) r^j]$ as the heat conduction vanishes for $r > r_e$. As can be seen, the outer velocity field corresponds in a first approximation to the incompressible flow induced by a volumetric source with strength $q/(j+1)$.

The hot kernel is separated from the outer gas by a thin transitional layer, where $T'/T'_o \sim O(1)$, of characteristic thickness $\varepsilon^{1/2}$. When the outer temperature remains constant, as occurs in the near-isobaric case for which $T' = T'_o$ for $r' > r'_e$, the solution for the temperature in the transition layer admits a self-similar description in terms of the local coordinate $y = (r_e - r)/(\varepsilon^{1/2}\delta)$, where the function $\delta(t)$ is that given in (3.9) with $p_e = 1$. The resulting profile, which was determined by Sánchez *et al.* (2003), can be obtained by integrating $-(1-\sigma) y T_y/(1+\sigma) + T^\sigma T_y^2 = T(T^\sigma T_y)_y$, which corresponds to (5.2) written in terms of the rescaled variables y and $T = T'/T'_o$. The boundary condition $T(-\infty) = 1$ corresponds to matching with the outer temperature $T' = T'_o$, while the boundary condition $T(\infty) \to y^{2/(\sigma+1)}$ follows from matching with the asymptotic behaviour of the hot-core temperature profile near the apparent contact surface.

5.2. *Self-similar thermal waves*

When the heating rate q varies with time with a power-law dependence, the thermal wave has a self-similar description. The similarity variable $\eta = r/\tau^{(\alpha+1)/(j+1)}$ follows from measuring the length with the instantaneous location of the contact surface $r_e = \tau^{(\alpha+1)/(j+1)}$, determined from (5.1) with $q = (1+\alpha)\tau^\alpha$, where the exponent α must be larger than -1 for the heat release to be finite and where the factor $(1+\alpha)$ must be included to satisfy the integral constraint $\int_0^1 q \, \mathrm{d}\tau = 1$. By introducing the similarity function $F(\eta) = \tau^{-(2\alpha - j + 1)/[(j+1)(\sigma+1)]} \Theta$ the problem reduces to that of integrating

$$\frac{2\alpha - j + 1}{(\alpha+1)(\sigma+1)} F - \eta F_\eta - \frac{F^2}{\eta^j} \left[\frac{1}{F} \left(1 + \frac{j+1}{\alpha+1} \eta^j F^\sigma F_\eta \right) \right]_\eta = 0 \tag{5.6}$$

with the boundary conditions

$$\left.\begin{array}{ll} \eta \to 0: & (1+\alpha)+(j+1)\eta^j F^\sigma F_\eta = 0, \\ \eta = 1: & F = 0. \end{array}\right\} \tag{5.7}$$

Results of integrations of this similarity problem with $\sigma = 0.5$ and different values of α are presented in figure 4. The profiles $H(\eta)$ shown in the figure as symbols pertain to non-isobaric self-similar solutions of the thermal wave with constant heating rate, to be developed below. Note that the profiles $\alpha = 0$, included here for completeness of the presentation, were originally given, in a slightly different notation, in Clarke *et al.* (1984) (for $j = 0$) and Sánchez *et al.* (2003) (for $j = 1$ and $j = 2$). As a final remark concerning these similarity solutions, it should be noted that the condition that the temperature in the thermal wave be sufficiently larger than T'_o, $\Theta^{\sigma+1} \gg (t'_d/t'_c)$, is a necessary requirement for the validity of the front solution. From the definition of F, it is clear that this condition is always satisfied if $\alpha \leqslant (j-1)/2$, while a front solution only develops for $\tau \gg (t'_d/t'_c)^{(j+1)/(2\alpha-j+1)}$ when $\alpha > (j-1)/2$.

5.3. *Near-isobaric post-heating evolution*

The period of heat deposition ends at $\tau = 1$, when the contact surface is located at $r_e = 1$. The contact surface remains at $r_e = 1$ for $\tau > 1$, when the temperature monotonically decreases within the hot pocket, where the gas starts moving towards the source, whereas the cold fluid located at $r > 1$ remains stagnant in first approximation. Note that this value $r'_e = r'_h$ for the final location of the contact surface follows directly from the definition (1.1), as can be seen by introducing $T' = T'_o$ for $r' > r'_e$ and $T' \gg T'_o$ for $r' < r'_e$ into the energy balance (1.5). Since in this near-isobaric case the amount of energy carried away from the hot kernel by the pressure wave is negligibly small, all of the energy deposited remains within the hot pocket for $t'_c \gg t' > t'_d$, with a distribution given in terms of the function h by $h = r^{j+1}$ for $r \leqslant 1$ and $h = 1$ for $r > 1$. This front-like description for the thermal wave eventually loses accuracy for times of order t'_c, when the temperature in the hot pocket becomes of the order of T'_o.

The evolution of the temperature after the source has been turned off at $\tau = 1$ is determined from the problem

$$\Theta^{-1}\left(\Theta_\tau + \Theta^\sigma \Theta_r^2\right) = r^{-j}(r^j \Theta^\sigma \Theta_r)_r, \qquad \left.\begin{array}{ll} \tau = 1: & \Theta = \Theta_d, \\ \tau > 1: & \begin{cases} r = 0: & \Theta_r = 0, \\ r = 1: & \Theta = 0, \end{cases} \end{array}\right\} \tag{5.8}$$

obtained by rewriting (5.2) and (5.3) with $q = 0$ and $r_e = 1$. The initial profile $\Theta_d(r)$, which must be computed by integrating (5.2) for $0 < \tau < 1$, becomes simply $\Theta_d = F(r)$ when the solution in the deposition period is of the similarity form investigated previously.

The initial profile $\Theta_d(r)$ remains initially unperturbed, except in the near-source region. The singular temperature distribution encountered for the point and line sources near the origin, whose leading-order behaviour is indicated in (5.4), evolves after the deposition period to give a finite peak temperature $\Theta = \Theta_s(\bar{\tau})$ at the source for $\bar{\tau} = \tau - 1 > 0$. In this near-source region, the effect of convection is negligible, so that the solution is given by a linear balance between accumulation and conduction that determines the initial evolution of the local temperature profile, which can be combined with the unperturbed outer solution Θ_d to provide a uniformly valid description for the temperature profile at $\bar{\tau} \ll 1$. For instance, for the line source the

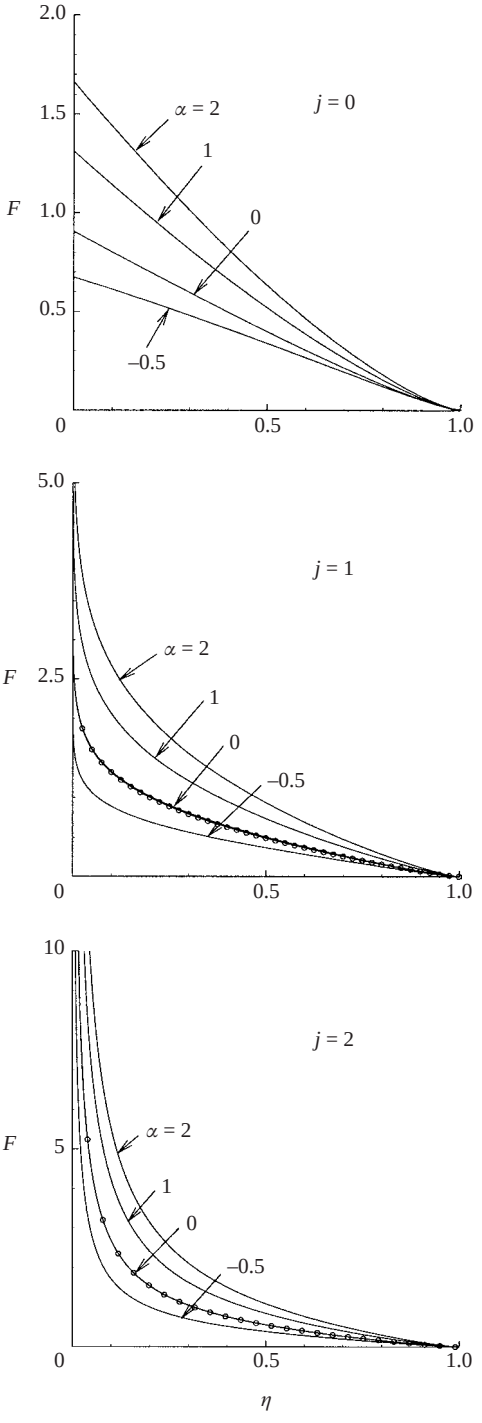

FIGURE 4. The self-similar profiles $F(\zeta)$, obtained with $\sigma = 0.5$ for different values of α; symbols represent the similarity function $H(\eta)$ defined below (6.8) for the point and line source.

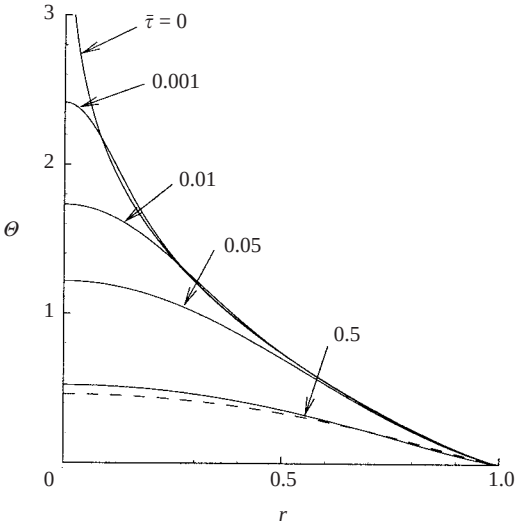

FIGURE 5. The solid lines represent temperature profiles obtained by integration of (5.8) with $\sigma = 0.5$ and with the initial self-similar profile $\Theta_d = F$ corresponding to $q = 2\tau$, while the dashed line is the asymptotic description corresponding to $\tau \gg 1$ evaluated at $\bar{\tau} = 0.5$.

analysis of the near-source region, of characteristic size $(\bar{\tau} \ln \bar{\tau}^{-1})^{1/2}$, provides

$$\Theta^{\sigma+1} = \Theta_d^{\sigma+1} - \frac{(\sigma+1)q_d}{4} E_1\left(\frac{r^2}{(\sigma+1)q_d \bar{\tau} \ln \bar{\tau}^{-1}}\right) \tag{5.9}$$

for the temperature profile, where E_1 is the exponential integral function and q_d is the value of the heating rate at $\tau = 1$. The analysis also gives the initial evolution of the source temperature

$$2\Theta_s^{\sigma+1}/[(\sigma+1)q_d] = -\tfrac{1}{2} \ln[(\sigma+1)q_d \bar{\tau} \ln \bar{\tau}^{-1}] + \gamma_1/2, \tag{5.10}$$

where γ_1 is Euler's constant. Equation (5.9) can be evaluated at $\bar{\tau} \ll 1$ to give a singularity-free initial temperature profile for integration of (5.8). Results corresponding to $\sigma = 0.5$ are shown in figure 5, where the initial profile is that produced by a linearly increasing heating rate $q = 2\tau$.

For $(\varepsilon t_d)^{-1} \gg \tau \gg 1$, the scaled temperature decreases to values of order $\tau^{-1/(\sigma+1)}$, as can be seen from a straightforward order-of-magnitude analysis of (5.8). This long-time behaviour admits a self-similar description, independent of the deposition period, in terms of the rescaled variable of order unity $G(r) = \tau^{1/(\sigma+1)}\Theta$, which is determined from the solution of the problem

$$\frac{1}{\sigma+1} + \frac{G}{r^j}(r^j G^{\sigma-1} G_r)_r = 0; \quad G_r(0) = G(1) = 0. \tag{5.11}$$

Numerical integration is in general required to provide the similarity profile G, although some explicit analytic solutions are available for the above problem for particular values of σ, i.e. when $\sigma = 0$, $G = (2/\pi^2)\sin^2[\pi(1-r)/2]$ and $G = (1-r^2)^2/8$ for $j = 0$ and $j = 1$, respectively. The profiles of G computed with $\sigma = 0.5$ are shown in figure 6 for the three geometrical configurations. The self-similar profile $\Theta = \tau^{-1/(\sigma+1)}G(r)$ corresponding to the line source is compared in figure 5 with the numerical results for $\bar{\tau} = 0.5$, indicating that the asymptotic solution for $\tau \gg 1$ already provides an accurate description for the temperature profile for values of $\tau - 1$ of

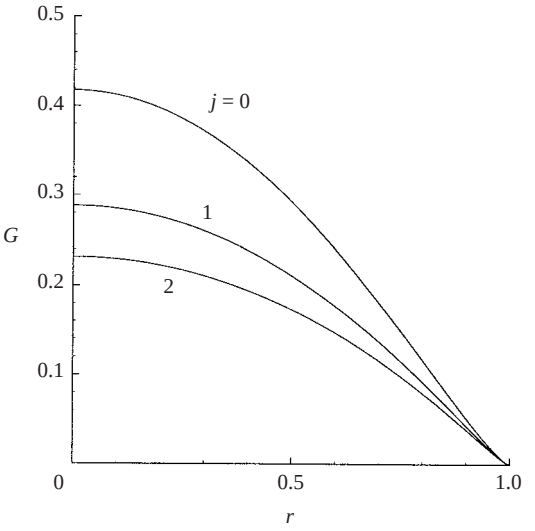

FIGURE 6. The self-similar profiles $G(r)$ obtained with $\sigma = 0.5$.

order unity. Note that the self-similar solution $\Theta = \tau^{-1/(\sigma+1)}G(r)$ holds for times in the intermediate range $t'_d \ll t' \ll t'_c$, when the temperature in the hot pocket remains much larger than the outer unperturbed temperature T'_o. Further evolution requires consideration of the distinguished regime $t' \sim t'_c$ with $T' \sim T'_o$, yielding the problem written below in (7.2) that uses the profile G to construct the initial temperature profile.

6. External energy sources with $t_d \sim O(1)$

When the deposition time t'_d is of order t'_a, i.e. $t_d \sim O(1)$, the cold fluid displaced by the contact surface moves with a characteristic velocity of the order of the velocity of sound, inducing changes in the non-dimensional pressure of order unity for $r > r_e$. In that case, the accumulation of internal energy in the inner conductive region, i.e. the first term in (3.7), can no longer be neglected, and the solution for the thermal wave becomes coupled to that of the outer compressible flow, which needs to be studied to determine the evolution of $r_e(t)$ and $p_e(t)$. The solution necessitates numerical integration of the Euler equations with boundary conditions given in (3.6), (3.7) and (3.10), with (3.7) reducing to (3.11) for $t > t_d$. The functions $r_e(t)$ and $p_e(t)$ determined in this way can then be used to solve for the thermal wave by integrating the problem displayed in (3.4) and (3.5). We investigate below the different stages following the application of the energy source, starting with the deposition period corresponding to $0 < t' < t'_d$, when the energy source is supplying heat at a given rate $q'(t')$. Appropriate dimensionless variables will be introduced for this heating period, during which the characteristic scales are related to the heating rate rather than to the total amount of energy deposited. Before treating in detail the flow induced by point and line sources with constant heating rate, we review briefly the self-similar solutions available.

6.1. *Self-similar heat propagation*

Self-similar solutions exist for the heat deposition period for heating rates with a power-law dependence on time of the form $q' \propto t'^j$, when both the shock wave and

the contact surface move with constant velocity. The outer flow corresponds to that induced by a moving piston ($j=0$), an expanding cylinder ($j=1$) or an expanding sphere ($j=2$), moving with a constant velocity $\mathrm{d}r'_e/\mathrm{d}t'$, which is related to the heating rate through the energy balance (3.7) evaluated with $\mathrm{d}p_e/\mathrm{d}t=0$

$$p_e \dot{r}_e^{\,j+1} = \bar{q}, \tag{6.1}$$

where $\bar{q}=(q'/t'^j)/[2^j\pi^{\delta_j}\rho'_o c_p T'_o(p'_o/\rho'_o)^{(j+1)/2}]$ is a dimensionless measure of the heating rate. The case of constant-rate heat deposition from a planar source, studied by Clarke *et al.* (1984), is particularly simple, in that the flow between the contact surface (the piston) and the shock wave is uniform, with a pressure $p_e=p_s$ that can be easily computed by equating the velocity for the shocked gas, given in the second equation (3.10), to the velocity of the contact surface obtained from (6.1). The solutions for the line source with linearly increasing heating rate and for the point source with quadratically increasing heating rate are somewhat more involved; they still make use of (6.1) to relate the piston velocity to the heating rate, but necessitate integration of the Euler equations written for the similarity coordinate r/t to find the pressure at the contact surface p_e for a given value of $\dot{r}_e$, as done by Taylor (1946) for the expanding sphere. Values of $\dot{r}_e$ and $\dot{r}_s$ obtained following this procedure for $\gamma=1.4$ with different values of the heating rate $\bar{q}$ are given in figure 7 for both the line and point sources. As can be seen, $\dot{r}_e\to(\bar{q})^{1/(j+1)}$ and $\dot{r}_s\to\gamma^{1/2}$ when $\bar{q}\ll 1$, which corresponds to the limit of near-isobaric heating. The corresponding outer acoustic solution is described in Deshaies & Clavin (1979) for $j=2$. For completeness, sample profiles of pressure and temperature obtained with $\bar{q}=(0.1, 1, 4)$ are also exhibited in the figure; the interested reader should consult Taylor (1946) for extensive calculations of the expanding sphere, to be used in connection with (6.1) for calculating the self-similar solution for the point source for other values of $\bar{q}$.

The self-similar description for the outer inviscid flow when $q'\propto t'^j$ is accompanied by a self-similar solution for the inner conductive core. Since the pressure does not vary with time, the resulting thermal wave can be related to the family of self-similar near-isobaric fronts identified above, yielding

$$T'/T'_o=\left[q'\Big/\left(2^j\pi^{\delta_j}k_o T'_o r'^{\,j-1}_e\right)\right]^{1/(\sigma+1)}F(\eta), \tag{6.2}$$

where the normalized coordinate $\eta=r'/r'_e$ is scaled with the location of the contact surface $r'_e=\dot{r}'_e t'$ and the similarity function F is that shown in figure 4 for $\alpha=j$.

6.2. *The outer inviscid compressible flow for a constant heating rate*

The flow structure is not self-similar for heating rates different from $q'\propto t'^j$, so that for the family of power-law rates $q'\propto t'^\alpha$, $\alpha>j$ leads to accelerating flows with leading shocks of increasing strength, while the flows show the opposite behaviour for $\alpha<j$, and are characterized initially by the appearance of a strong shock wave. As a relevant example of the latter type of solution, we investigate below the flow induced by a line or point source with a constant heating rate.

To study the deposition period, it is convenient to introduce as scales for time and length those associated with the constant heating rate $q'=q'_o$. As can be inferred from (3.7), this rate defines a characteristic time, t'_o, obtained from the energy balance

$$\frac{2^j\pi^{\delta_j}}{j+1}\rho'_o c_p T'_o(p'_o/\rho'_o)^{(j+1)/2}=\frac{q'_o}{t'^j_o}, \tag{6.3}$$

for which the velocity of the contact surface has decreased to a value of the order of the sound velocity, giving pressure increments of the order p'_o. Using this characteristic

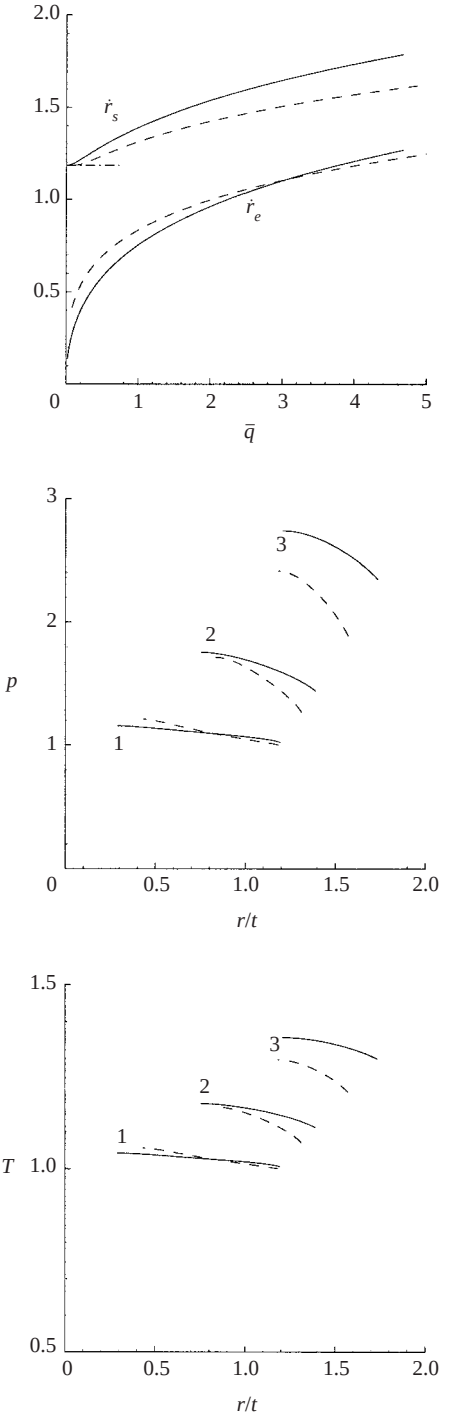

FIGURE 7. The variation of $\dot{r}_s$ and $\dot{r}_e$ with the heating rate $\bar{q}$ obtained with $\gamma = 1.4$ for $j = 1$ (solid lines) and $j = 2$ (dashed lines), along with the self-similar profiles of pressure and temperature obtained with $\bar{q} = 0.1$ (1), $\bar{q} = 1$ (2) and $\bar{q} = 4$ (3).

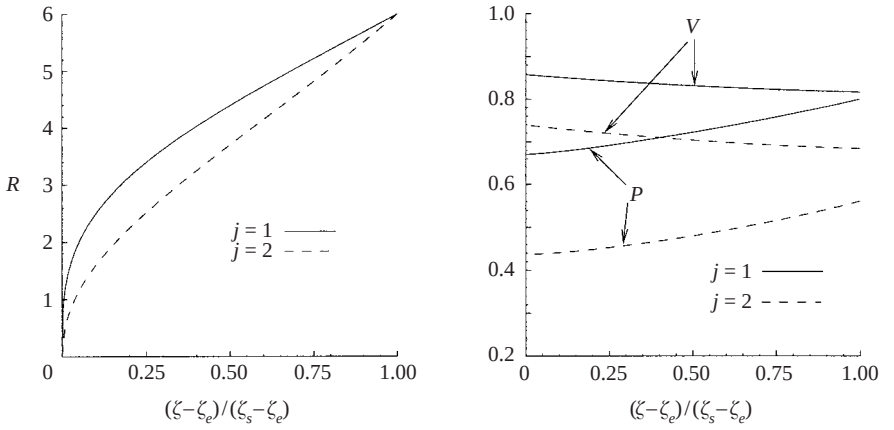

FIGURE 8. The self-similar profiles $R(\zeta)$, $P(\zeta)$ and $V(\zeta)$ obtained with $\gamma = 1.4$ for $j = 1$ (solid lines) and $j = 2$ (dashed lines).

time, and its associated length $r'_o = (p'_o/\rho'_o)^{1/2} t'_o$, in defining the alternative non-dimensional coordinates $\hat{r} = r'/r'_o = t_d^{1/j} r$ and $\hat{t} = t'/t'_o = t_d^{1/j} t$, reduces (3.6) and (3.7) to

$$v = \frac{\mathrm{d}\hat{r}_e}{\mathrm{d}\hat{t}} = \dot{r}_e, \qquad \frac{\hat{r}_e^{\,j+1}}{\gamma} \frac{\mathrm{d}p_e}{\mathrm{d}\hat{t}} + p_e \frac{\mathrm{d}\hat{r}_e^{\,j+1}}{\mathrm{d}\hat{t}} = 1. \tag{6.4}$$

The solution for the outer flow involves numerical integration of the Euler equations supplemented with the jump conditions (3.10) at $\hat{r} = \hat{r}_s$ and (6.4) at $\hat{r} = \hat{r}_e$, yielding a problem that depends only on the parameter γ, i.e. the deposition time t_d enters only when defining the end of the deposition period, which corresponds in this alternative formulation to the instant $\hat{t} = t_d^{(j+1)/j}$.

An infinitely strong shock forms initially following the application of a constant-rate source from a line or point, source, giving a singular behaviour for $\hat{t} \ll 1$, which was first analysed by Rogers (1958), that needs to be computed to provide the initial profiles of density, pressure and velocity. To describe this initial period, we write the Euler equations in terms of the similarity variables of order unity, $P(\zeta) = \hat{t}^{2j/(j+3)} p$, $R(\zeta) = \rho$ and $V(\zeta) = \hat{t}^{j/(j+3)} v$, along with the similarity coordinate $\zeta = \hat{r}/\hat{t}^{3/(j+3)}$. Integrating the resulting system of ordinary differential equations with boundary conditions at the contact surface

$$\zeta = \zeta_e: \quad V = \frac{3}{j+3}\zeta, \quad \frac{\zeta^{j+1}}{(j+3)\gamma}\{[3\gamma(j+1) - 2j]P - 3\zeta P_\zeta\} = 1 \tag{6.5}$$

and at the leading shock

$$\zeta = \zeta_s: \quad R = \frac{\gamma+1}{\gamma-1}, \quad V = \left(\frac{2P}{(\gamma+1)}\right)^{1/2}, \quad \frac{3}{j+3}\zeta = \left(\frac{(\gamma+1)P}{2}\right)^{1/2} \tag{6.6}$$

determines for a given value of γ the self-similar profiles $P(\zeta)$, $V(\zeta)$ and $R(\zeta)$, along with the values of ζ_s and ζ_e. The solution corresponding to $\gamma = 1.4$ is shown in figure 8. In this case, the locations of the contact surface and of the shock wave are $\zeta_e = (1.1434, 1.2311)$ and $\zeta_s = (1.3066, 1.3673)$ for $j = (1, 2)$, respectively, while the corresponding boundary pressures are $P_e = (0.6705, 0.4363)$ and $P_s = (0.8003, 0.5609)$. The density profiles are seen to vanish at the contact surface, approaching the boundary with a local solution of the form $R \propto (\zeta - \zeta_e)^{1/(3\gamma-1)}$ if $j = 1$ and

$R \propto (\zeta - \zeta_e)^{4/(9\gamma-4)}$ if $j=2$. To understand this behaviour, note that each fluid particle conserves its entropy after crossing the shock. The fluid particles at $\zeta=\zeta_e$, which at the initial instant cross the infinitely strong shocks, must therefore maintain an infinitely large entropy as they expand, which can only be achieved with an infinite temperature and, therefore, a vanishing density. This singular behaviour is absent in the self-similar solutions corresponding to $q' \propto t'^j$, for which the application of the heating rate results in a shock wave of finite constant strength, so that the resulting temperature remains finite at the contact surface. Note also that, as a consequence of the vanishing density, a zero pressure gradient $P_\zeta=0$ is needed to accelerate the fluid located at $\zeta=\zeta_e$, thereby simplifying (6.5).

The self-similar solution for $\hat{t}\ll 1$, evaluated at $\hat{t}=10^{-5}$ $(j=1)$ and at $\hat{t}=10^{-4}$ $(j=2)$, was used as initial condition to integrate the Euler problem for the outer compressible flow for $\gamma=1.4$. The resulting values of the velocity and location of the contact surface and of the shock wave are plotted in figure 9, along with the associated boundary pressures. For completeness, the figure includes comparisons with the asymptotic behaviour for $\hat{t}\ll 1$. As expected, the numerical solution shows departures from the asymptotic results as the rescaled time $\hat{t}$ increases to values of order unity. The pressure decreases for increasing values of $\hat{t}$, so that the near-isobaric limit $p=1$ is approached for $\hat{t}\gg 1$, when the velocity of the contact surface is given by $\dot{r}_e \simeq \hat{t}^{-j/(j+1)}/(j+1)$, as can be deduced from (6.4), and the shock wave becomes a weak discontinuity moving with a velocity slightly above the velocity of sound, $\dot{r}_s \simeq \gamma^{1/2}$. Sample profiles of temperature and pressure corresponding to different values of $\hat{t}$ are given in figure 10 for the line source. These profiles constitute the initial condition for studying the flow evolution after the source is switched off at $\hat{t}=t_d^{(j+1)/j}$, a problem addressed in the following section.

6.3. *The conductive thermal wave for a constant heating rate*

The same rescaled variables $\hat{t}$ and $\hat{r}$ can be used, together with a rescaled temperature $\hat{\theta}=\{\alpha_o/[(p_o'/\rho_o')^{1/2}r_o']\}^{1/[j(\sigma+1)]}(T'/T_o')=t_d^{1/[j(\sigma+1)]}\theta$, to write equations (3.4) and (3.5) in the form

$$\frac{\partial}{\partial \hat{t}}\left(\frac{p_e}{\hat{\theta}}\right)+\frac{1}{\hat{r}^j}\frac{\partial}{\partial \hat{r}}\left[\frac{1}{\hat{\theta}}\left(\frac{1}{(j+1)}-\frac{\hat{r}^{j+1}}{(j+1)\gamma}\frac{\mathrm{d}p_e}{\mathrm{d}\hat{t}}+\hat{r}^j\hat{\theta}^\sigma\frac{\partial\hat{\theta}}{\partial\hat{r}}\right)\right]=0 \tag{6.7}$$

and

$$\begin{aligned}&\hat{t}=0: \quad \hat{\theta}=0,\\ &\hat{t}>0: \quad \left\{\begin{array}{ll}\hat{r}\to 0: & (j+1)\hat{r}^j\hat{\theta}^\sigma\,\partial\hat{\theta}/\partial\hat{r}=-1,\\ \hat{r}=\hat{r}_e: & \hat{\theta}=0,\end{array}\right\}\end{aligned} \tag{6.8}$$

which can be integrated, with use made of the functions $p_e(\hat{t})$ and $\hat{r}_e(\hat{t})$ determined above, to provide the variation with time of the thermal wave for a given value of σ. Self-similar solutions exist for both $\hat{t}\ll 1$ and $\hat{t}\gg 1$ which can be obtained by introducing the normalized coordinate $\eta=\hat{r}/\hat{r}_e$, with $\hat{r}_e=\zeta_e\hat{t}^{3/(j+3)}$ for $\hat{t}\ll 1$ and $\hat{r}_e=\hat{t}^{1/(j+1)}$ for $\hat{t}\gg 1$. As seen above in figure 9, the pressure approaches the ambient value $p_e=1$ for $\hat{t}\gg 1$, yielding a near-isobaric thermal wave of the form $\hat{\theta}=\hat{t}^{-(j-1)/[(j+1)(\sigma+1)]}F(\eta)$, where F, depicted in figure 4, is determined from integrating (5.6) and (5.7) with $\alpha=0$. It is interesting that the solution for $\hat{t}\ll 1$ can be expressed in terms of the same family of similarity functions. Introducing

$$\hat{\theta}=\left[\zeta_e\hat{t}^{3/(j+3)}\right]^{-(j-1)/(\sigma+1)}H, \tag{6.9}$$

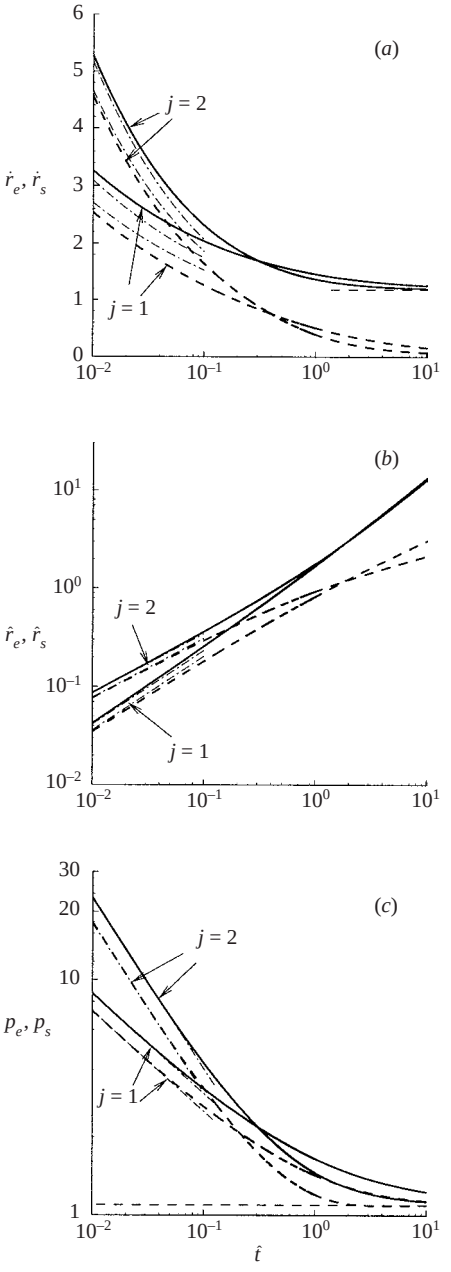

FIGURE 9. The variation with time of the velocity (*a*), location (*b*) and pressure (*c*) of the contact surface (dashed lines) and of the shock wave (solid lines) obtained during the deposition period with constant heating rate and $\gamma = 1.4$. The dot-dashed lines represent the asymptotic behaviours for $\hat{t} \ll 1$.

and taking into account the result $\zeta_e^{j+1} P_e = \gamma(j+3)/[3\gamma(j+1) - 2j]$, which follows from (6.5) with $P_\zeta = 0$, reduces (6.7) and (6.8) to the similarity problem given above in (5.6) and (5.7), with $\alpha = 0$ and with the numerical factor $(2\alpha - j + 1)/[(\alpha + 1)(\sigma + 1)]$ affecting F being replaced with $2(\gamma - 1)/(3\gamma - 1)$ for $j = 1$ and $-[9\gamma - 12(\sigma + 1)$

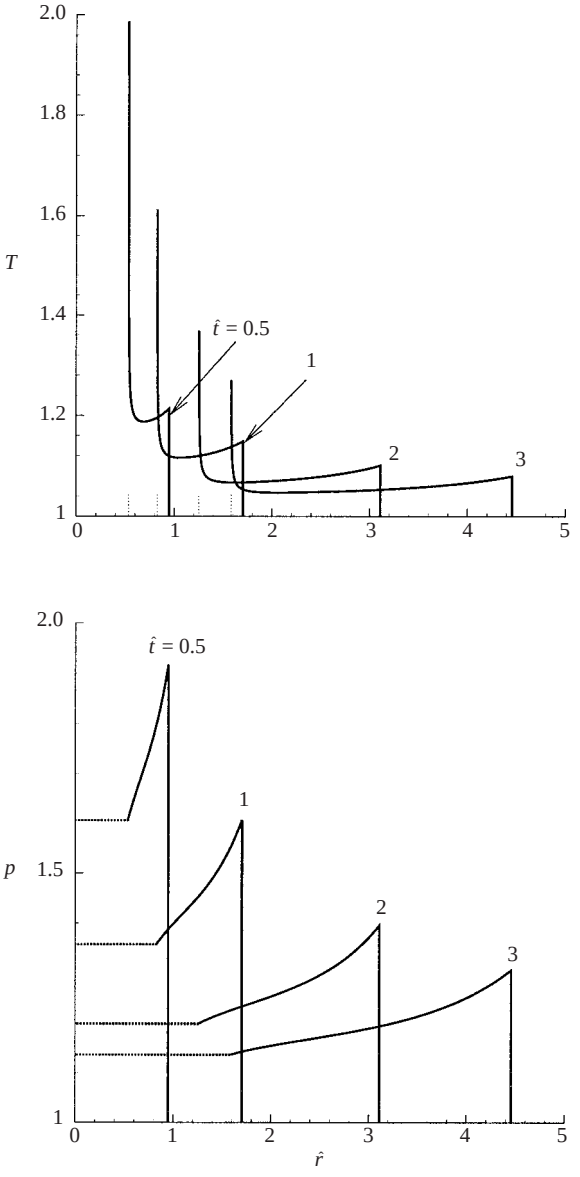

FIGURE 10. Temperature and pressure profiles induced in the outer region by a line source of constant heating rate.

$(\gamma - 1)]/[(9\gamma - 4)(\sigma + 1)]$ for $j = 2$. The self-similar profiles $H(\eta)$, obtained with $\gamma = 1.4$ and $\sigma = 0.5$, are shown as symbols in figure 4 for the point and line sources. As can be seen, in both cases the differences with the corresponding profiles F with $\alpha = 0$ are imperceptible.

Temperature profiles determined by integration of (6.7) and (6.8) for the spherical thermal wave with $\sigma = 0.5$ are shown in figure 11. For comparison, we include the asymptotic behaviours at small and large times. Cylindrical thermal waves were also computed. In that case, the asymptotic behaviours reduce to $\hat{\theta} = F(\eta)$ for $\hat{t} \gg 1$ and to $\hat{\theta} = H(\eta)$ for $\hat{t} \ll 1$. It is interesting to note that, since the functions F and H

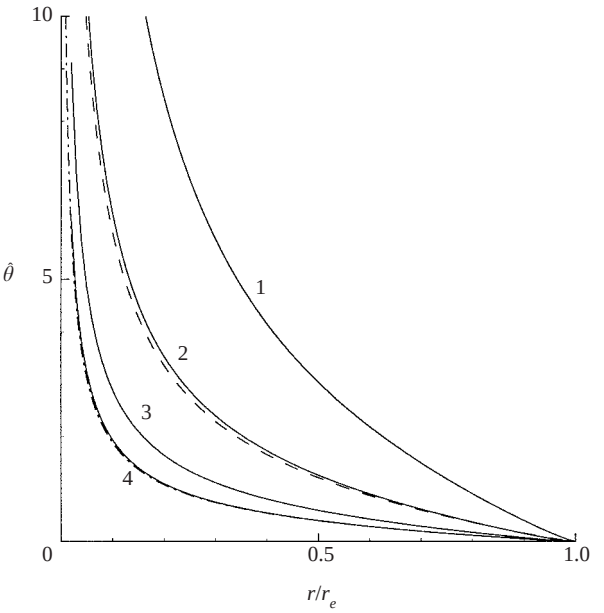

FIGURE 11. Solid lines represent profiles of $\hat{\theta}$ at $\hat{t}=0.01$ (1), $\hat{t}=0.1$ (2), $\hat{t}=1$ (3) and $\hat{t}=5$ (4), obtained for the point source from numerical integration of (6.7) and (6.8) with $\sigma=0.5$; the profile at $\hat{t}=0.1$ is compared with the asymptotic prediction for $\hat{t}\ll 1$, while the profile at $\hat{t}=5$ is compared with the asymptotic prediction for $\hat{t}\gg 1$.

are practically identical, the shape of the resulting temperature profiles obtained by integration of (6.7) and (6.8) for the line source does not change appreciably in time when, as in figure 11, the normalized coordinate r/r_e is used.

7. Post-heating evolution for $t > t_d$

After the source is switched off, the evolution of the hot fluid volume $r < r_e$ is globally isentropic, as stated in (3.11). In the absence of a driving mechanism, the rate of expansion of the hot core diminishes, leading to a rapid decrease of the pressure p_e. This is illustrated in figures 12 and 13, where we show the flow evolution after a line source is switched off at $t_d=0.1$. The results correspond in particular to sources with a linearly increasing heating rate and with a constant heating rate, the two cases investigated in the previous section. As can be seen, there is an expansion wave that propagates outwards, reaching the shock wave at a later instant. Both the contact surface and the shock wave decelerate, the former to occupy a final location $r_e=r_a$ and the latter to eventually become a negligibly weak wave of the acoustic type. Outside the heat conduction core, the solution for $t\gg 1$ shows an interior region of stagnant gas at atmospheric pressure, where the temperature has already attained a constant distribution $T_a(r)$. As in the case of instantaneous heat deposition discussed above, the near-acoustic wave travelling outwards shows a characteristic structure with a rarefaction region of reverse flow lagging behind the compressed gas. As before, no development of secondary discontinuities was found in the numerical computations for the range of times considered, suggesting that, as in the case of instantaneous deposition studied by Okhotsimskii & Vlasova (1962), a second shock develops from the rarefaction region only for $t\gg 1$.

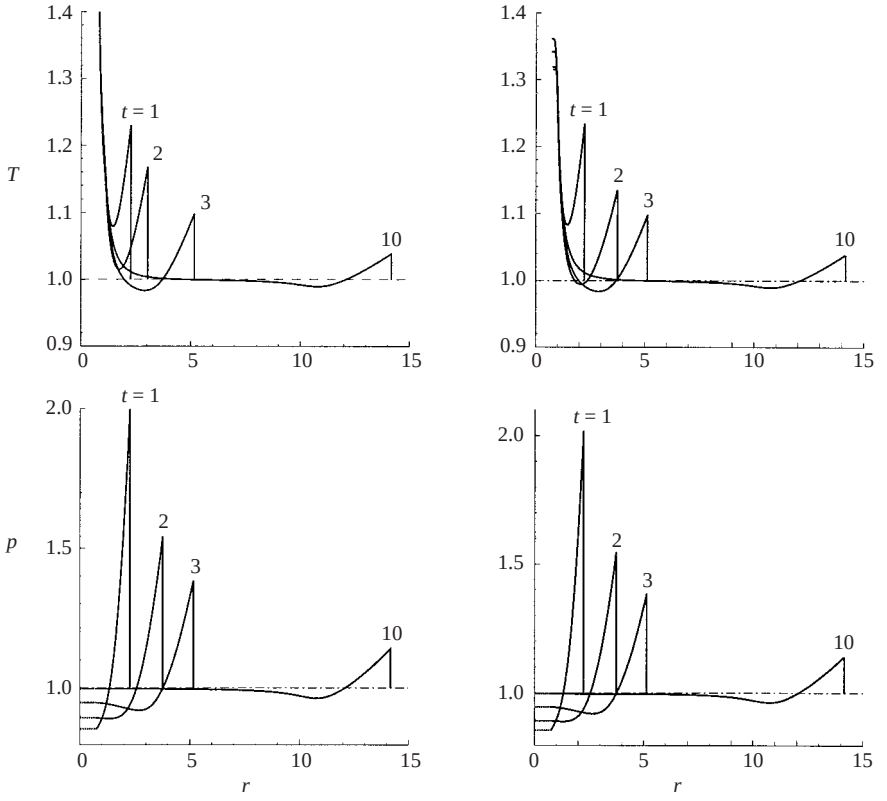

FIGURE 12. Post-heating evolution of the temperature and pressure for a line source with $t_d = 0.1$ and $\gamma = 1.4$. The left-hand plots correspond to a source of constant heating rate, while the right-hand plots correspond to a source of linearly increasing heating rate.

The velocity of the contact surface vanishes as the pressure settles to the ambient value $p = 1$ for $t \gg 1$, so that (3.11) gives the final asymptotic value of $r_e = r_a$ for given values of r_e and p_e at $t = t_d$. The resulting value of r_a, a function of the deposition rate, is in the range $0 \leqslant r_a \leqslant 1$, where the lower bound $r_a = 0$ is approached according to $r_a \sim t_d^{2(\gamma-1)/[\gamma(j+3)]}$ for $t_d \ll 1$, while the upper bound $r_a = 1$ corresponds to isobaric deposition ($t_d = \infty$). It is possible to compute r_a in some cases of interest. For instance, if the heat is released with a rate $q' \propto t'^j$, use of (6.1) yields $r_a = (\dot{r}_e t_d)^{(\gamma-1)/\gamma}$, where the constant contact-surface velocity during the heating period $\dot{r}_e$ is given in figure 7 as a function of the dimensionless heating rate $\bar{q} = 1/t_d^{j+1}$. It is also possible to compute r_a for a line or point source of constant heating rate when $t_d \ll 1$. In that case, the analysis of the limit $\hat{t} \ll 1$ yields $r_e = \zeta_e t_d^{2/(j+3)}$ and $p_e = P_e t_d^{-2(j+1)/(j+3)}$ at the end of the deposition period. Introducing these values into (3.11) yields $r_a = \zeta_e P_e^{1/[\gamma(j+3)]} t_d^{2(\gamma-1)/[\gamma(j+3)]}$ for the final contact-surface location.

The contact surface divides the hot gas into two regions: an inner region for $r < r_a$ where the gas was heated by conduction from the source and an outer region where the temperature has increased as a result of the shock wave heating. In the inner region, the evolution of the temperature for $t > t_d$ is qualitatively similar to that shown in figure 5, giving a profile that for $\varepsilon^{-1} \gg t \gg 1$ eventually approaches the asymptotic self-similar form

$$T_a = \left[r_a^2/(\varepsilon t)\right]^{1/\sigma+1} G(r/r_a) \quad \text{for} \quad r < r_a, \tag{7.1}$$

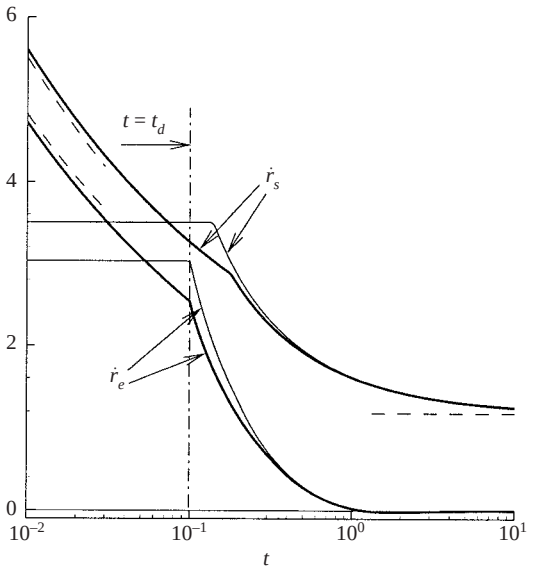

FIGURE 13. The velocities of the contact surface and of the shock wave for a line source with $t_d = 0.1$ and $\gamma = 1.4$. The thick lines correspond to a source of constant heating rate, while the thin lines correspond to a source of linearly increasing heating rate.

where the function G is plotted in figure 6. The associated fraction of energy stored up to the radius r is simply $h = r^{j+1}$ for $r \leqslant r_a$ as can be seen from (4.2) with $T_a \gg 1$, so that the relative amount of energy that remains in this inner hot region is r_a^{j+1}. The rest of the energy lies in the outer gas, with a final distribution that depends on the shock history through the entropy gain of each shocked fluid particle.

The numerical procedure for the calculation of T_a is analogous to that previosly delineated in § 4. The outer profiles of $T_a(r)$ and $h(r)$ corresponding to a line source are shown in figure 14 for different values of t_d and for the two heating rates of figures 12 and 13. The profile $T_a(r)$ corresponding to instantaneous heat deposition, given previously in figure 3, is included for completeness. The comparison with the profile $t_d = 0.01$ reveals that the finite deposition time influences significantly the asymptotic temperature profile even for very intense sources with $t_d \ll 1$. However, for this case $t_d = 0.01$ the function giving the stored energy fraction, $h(r)$, is practically indistinguishable from that shown in figure 3 for instantaneous heat deposition.

The profiles of h corresponding to a given t_d are very similar for the two heating rates, while larger differences are seen in the temperature profile as the contact surface is approached, a behaviour also observed in the temperature profiles of figure 12. For a linearly increasing heating rate, the constant finite strength of the shock wave during the deposition period results in a finite value of T_a at the contact surface. On the other hand, for the source of constant rate the shock wave formed initially is infinitely strong, thereby giving an infinite value for $T_a(r_a)$, with $T_a \propto (r - r_a)^{-2j/[3\gamma(j+1)-2j]}$ for $r - r_a \ll 1$. Note that this singularity would not be present if, as can be expected in realistic configurations, a finite time is required for the heating rate to increase from zero to a given constant value as the source is switched on at $t = 0$.

The temperature profile $T_a(r)$ given in (7.1) for $r < r_a$ and in figure 14 for $r > r_a$ is modified for times of order t_c'. With compressibility effects being negligible, the solution for this final stage depends on the combined effect of heat conduction

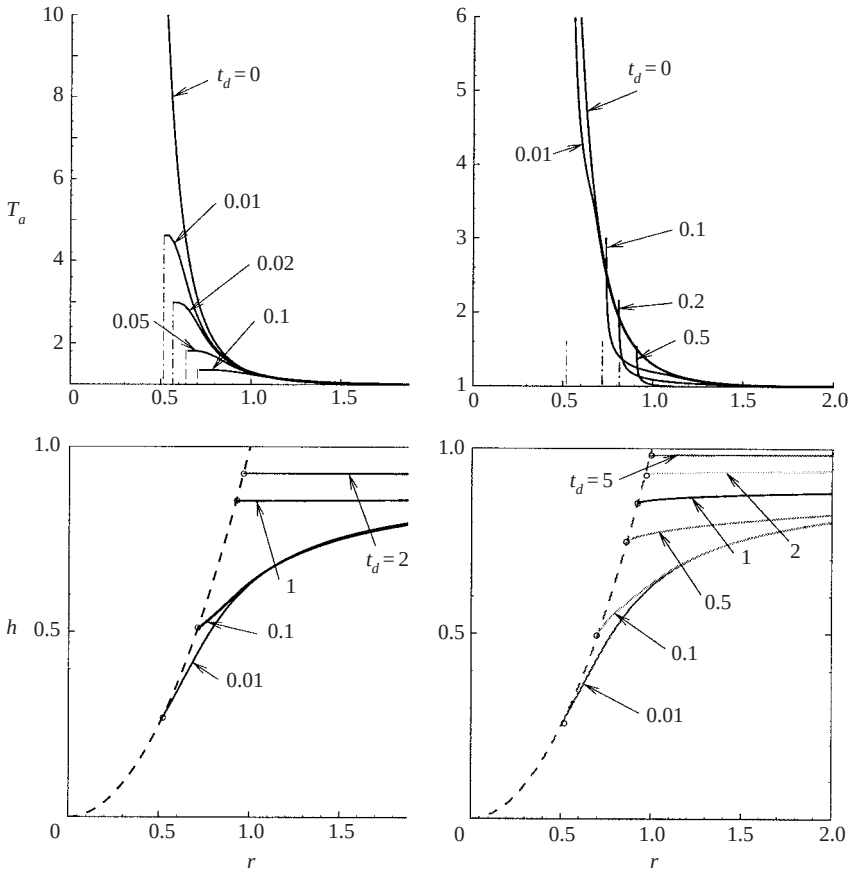

FIGURE 14. The profiles of T_a and h corresponding to a line source with a linearly increasing heating rate (left-hand plots) and with a constant heating rate (right-hand plots). The dashed line $h=r^2$ corresponds to the fraction of energy stored in the hot core, which is bounded by $r=r_a(t_d)$, defined by the circles in the figure.

towards the cold outer gas and inwards convection, necessary to replenish the low-density hot pocket. Starting from the continuity and energy conservation equations, and following the development leading to (3.4), produces in this case the heat problem

$$\frac{1}{T^2}\frac{\partial T}{\partial \varsigma}-\frac{1}{r^j}\frac{\partial}{\partial r}\left(r^j T^{\sigma-1}\frac{\partial T}{\partial r}\right)=0; \quad \begin{matrix} \varsigma=0: & T=T_a(r), \\ \varsigma>0: & \begin{cases} r=0: & \partial T/\partial r=0, \\ r\to\infty: & T=1, \end{cases} \end{matrix} \tag{7.2}$$

where use is made of the non-dimensional time of order unity $\varsigma=t'/t'_c=\varepsilon t$. Since the energy released during the deposition period remains in the flow field as an excess enthalpy, the solution for the temperature profile must satisfy the integral constraint $(j+1)\int_0^\infty (1-1/T)r^j\,\mathrm{d}r=1$, as obtained from a first quadrature of (7.2).

The heating rate applied during the deposition period enters this final conductive period through the initial temperature profile T_a, which is constructed by combining the asymptotic solution (7.1), evaluated at $\varepsilon t\ll 1$, with the outer profile shown in figure 14. For instantaneous heat deposition ($t_d\ll 1$) the hot kernel is negligibly small and the initial temperature distribution is that given in figure 3. The problem was addressed by Meerson (1989), who studied the initial near-source evolution for

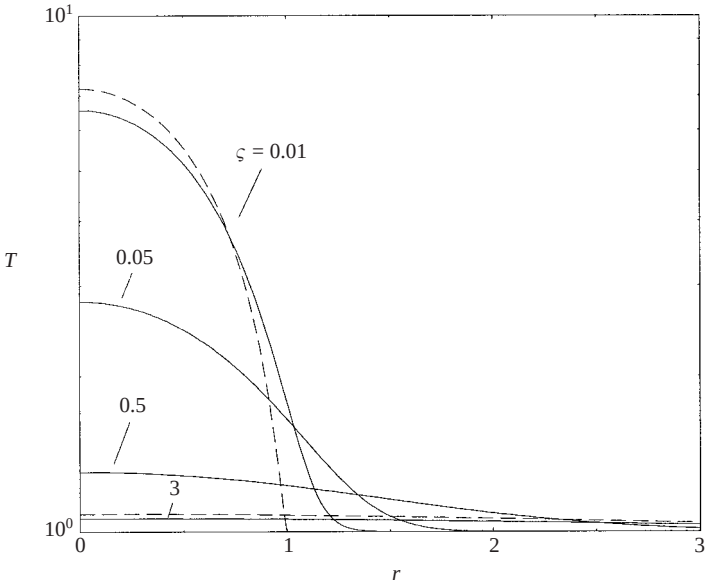

FIGURE 15. The conductive evolution of the temperature for $j=1$ for near-isobaric heat deposition from an energy source with $t_d \gg 1$; the dashed lines represent temperature profiles determined from the asymptotic behaviours at $\varsigma \ll 1$ and $\varsigma \gg 1$.

the spherical hot pocket. On the other hand, in the opposite limit of near-isobaric deposition $t_d \gg 1$, the temperature increment in the outer region is negligible, and the initial temperature reduces to

$$T_a = 1 + \varsigma^{-1/\sigma+1} G(r). \tag{7.3}$$

The associated solution to (7.2) is given in figure 15 for the line source. The profile (7.3) evaluated at $\varsigma = 0.001$ was used as initial condition in the integration. To illustrate the evolution of the solution for $\varsigma \ll 1$, the profile obtained numerically at $\varsigma = 0.01$ is compared in the figure with the initial profile (7.3).

The hot pocket continues evolving for times much larger than the conduction time, when the temperature and the density approach their ambient values. The small departures of the temperature from T'_o,

$$T - 1 = \frac{\varsigma^{-(j+1)/2}}{2^j (j+1)\,\Gamma\,\frac{1}{2}(j+1)} \exp\left(-\frac{r^2}{4\varsigma}\right), \tag{7.4}$$

are given by the self-similar constant-density solution (Carslaw & Jaeger 1959), where Γ represents the Gamma function (Abramowitz & Stegun 1965). As can be seen, the final temperature evolution depends only on the total amount of energy released E_j, which determines the scale r'_h used to define $r = r'/r'_h$ and $\varsigma = t'/(r'^2_h/\alpha_o)$. This long-time asymptotic prediction is compared in figure 15 with the profile obtained at $\varsigma = 3$ by integration of (7.2).

8. Conclusions

The present paper has investigated heat propagation in a gas from planar, line and point sources of size much smaller than the size r'_h of the region being heated.

Deposition times t'_d of the order of the relevant acoustic time $t'_a = r'_h/(p'_o/\rho'_o)^{1/2}$ are considered in the paper, a limit previously explored by Clarke *et al.* (1984) in their analysis of heating of a gas from a plane wall. As in the previous work, it is seen that heat conduction cooperates with convection to heat the gas surrounding the source, forming a nearly empty high-temperature kernel of uniform pressure. The boundary of this hot kernel acts as a contact surface that displaces the outer cold fluid, inducing velocities that are of the order of the unperturbed velocity of sound. This rapid displacement produces a shock wave that propagates outwards, increasing the temperature by a relative amount of order unity in a region of size comparable to that of the conductive hot kernel. Although our work has been restricted to symmetric configurations, the same two-region flow structure is present around non-symmetric energy sources, such as a line source of finite length, a problem that should be addressed in future work.

The ratio of the acoustic time to the conduction time ε, of the order of the characteristic Knudsen number of the reference state, has been taken as an asymptotically small parameter in formulating the governing equations for the two separate regions. Besides the distinguished limit $t'_d \sim t'_a$, particular consideration has been given to the limits of near-isobaric heat propagation, $t'_d \gg t'_a$, and instantaneous heat release, $t'_d \ll t'_a$, thereby complementing our previous investigation of the limit $t'_d \sim t'_c$ (Sánchez *et al.* 2003) . The different solutions arising in the different cases are summarized below, where the reader should remember that $t'_\lambda/t'_a \sim t'_a/t'_c = \varepsilon \ll 1$.

Instantaneous heat deposition ($t'_d \ll t'_a$)

(i) $t'_d \ll t' \ll t'_a$: the self-similar description of the initial blast wave is due to Sedov (1946) and Taylor (1950).

(ii) $t' \sim t'_a$: the evolution of the shock wave was first computed numerically by Goldstine & Neumann (1955) and Brode (1955) for $j = 2$ and by Korobeinikov & Chushkin (1966) for $j = (0, 1)$.

(iii) $t'_a \ll t' \ll t'_c$: the asymptotic distribution of temperature as the pressure settles everywhere to the ambient value, of interest for flame initiation studies, is given in figure 3.

(iv) $t' \sim t'_c$: the final conductive evolution is described by (7.2). The near-source initial evolution was given for the point source by Meerson (1989).

Two-region flow structure ($t'_d \sim t'_a$). There exists an inner hot kernel described by (3.4) and (3.5) and an outer inviscid compressible region, described by the Euler equations supplemented with (3.6), (3.7) and (3.10).

(i) $t' \ll t'_d$: for constant heating rate, the self-similar solution for the initial evolution of the outer flow, described by Rogers (1958), Freeman (1968), and Dabora (1972), is shown in figure 8, whereas the associated self-similar temperature profile in the hot core is given in (6.9).

(ii) $t' \leqslant t'_d$: there exist self-similar descriptions when $q' \propto t'^j$. For the outer flow, the solution, given in figure 7, corresponds to the flow induced by a constant-velocity piston, first described for $j = 2$ by Taylor (1946). The corresponding self-similar temperature profile in the hot core is given in (6.2). For a constant heating rate, the solution requires numerical integration, leading to the results shown in figures 9 and 10 for the outer region and in figure 11 for the inner region.

(iii) $t'_d < t' \sim t'_a$: the solution requires numerical computation, giving the evolution shown in figures 12 and 13.

(iv) $t'_a \ll t' \ll t'_c$: the temperature reaches a constant distribution in the outer region, shown in figure 14, while the temperature in the hot kernel reaches a self-similar profile given in (7.1), where the function G is plotted in figure 6.

(v) $t' \sim t'_c$: the final conductive evolution is described by (7.2).

Near-isobaric fronts ($t'_a \ll t'_d \ll t'_c$). The solution for the temperature in the hot kernel is described by (5.2) and (5.3).

(i) $t' < t'_d$: the front solutions admit a self-similar description for $q' \propto t'^{\alpha}$, which is given in figure 4. The solutions for a constant heating rate were first obtained by Clarke *et al.* (1984) ($j = 0$) and by Sánchez *et al.* (2003) ($j = 1, 2$).

(ii) $t'_d < t' \ll t'_c$: the solution requires numerical integration of (5.8), giving the evolution shown in figure 5.

(iii) $t'_d \ll t' \ll t'_c$: there exists a self-similar solution, (7.3), for the temperature, where the function G is plotted in figure 6.

(iv) $t' \sim t'_c$: the final conductive evolution is described by (7.2), with results given in figure 15.

As previously mentioned, our study has considered the heating period during which the source remains active, and also the post-heating evolution corresponding to $t' > t'_d$. For times much smaller than the conduction time $t'_c = r'^2_h/\alpha_o$, the hot kernel remains clearly distinct from the outer inviscid compressible region, so that the asymptotic temperature profile $T_a(r)$ encountered at times in the intermediate range $t'_a \ll t' \ll t'_c$ includes the self-similar solution (7.1) for $r < r_a$ and the constant distribution of figure 14 for $r > r_a$.

In summary, the results of our work are relevant for the calculation of the minimum ignition energy for deflagration initiation, a quantity of interest for premixed combustion devices and accidental explosion events. The previous numerical studies of Maas & Warnatz (1988) and Frendi & Sibulkin (1990) have indicated that ignition is more easily achieved with concentrated sources with deposition times sufficiently smaller than the conduction time. Under such conditions, the asymptotic temperature distribution $T_a(r)$ given above constitutes the appropriate initial condition for integration of the reactive conservation equations. To determine the minimum ignition energy E_m for a given value of t_d the integrations should consider initial temperature distributions corresponding to different E_j. Depending on the amount of energy deposited, either successful initiation of a self-sustained deflagration or ignition failure would be observed. The energy and temperature distributions of figure 14 allow us to anticipate the dependence of the minimum ignition energy on t_d. As shown in figure 14, for sources with $t_d \lesssim 1$ the shock wave that forms effectively distributes a fraction of the energy away from the source, in an extended region where the temperature increases only by a small relative amount. It can be expected that this mildly heated gas has only a limited effect on the ignition process, which is mainly controlled by the high-temperature kernel. Since the energy of this core is only a fraction r_a^{j+1} of the total energy deposited E_j, the resulting value of E_m decreases for increasing values of t_d. The smallest value of E_m will be associated with values of $t_d \gg 1$, corresponding to the intermediate range $t'_c \gg t'_d \gg t'_a$, when the shock wave produced during the deposition period is negligibly weak and all of the heat deposited appears concentrated in a neatly defined inner core of very high temperature, yielding the most favourable conditions for ignition. Clearly, the use of (7.3) as initial condition in calculations of E_m should be investigated in future work.

The authors would like to thank Professor J. H. S. Lee for interesting discussions on the subject. This research was supported by the Fifth Framework Programme of the European Commission under the Energy, Environment and Sustainable Development Contract No EVG1-CT-2001-00042 EXPRO and by the Spanish MCYT under project No DPI2001-4603-E. Vadim Kurdyumov gratefully acknowledges the financial support received from the Spanish Ministry of Education through contract # SAB2000-0169 during the development of this research.

REFERENCES

Abramowitz, A. & Stegun, M. 1965 *Handbook of Mathematical Functions*. Dover.

Brode, H. L. 1955 Numerical solution of spherical blast waves. *J. Appl. Phys.* **26**, 766–775.

Carrier, G. F., Fendell, F. E. & Marble, F. E. 1975 The effect of strain rate on diffusion flames. *SIAM J. Appl. Maths* **28**, 463–500.

Carslaw, H. S. & Jaeger, J. C. 1959 *Conduction of Heat in Solids*, 2nd edn. Oxford University Press.

Clarke, J. F., Kassoy, D. R., Meharzi, N. E., Riley, N. & Vasantha, R. 1990 On the evolution of plane detonations. *Proc. R. Soc. Lond.* A **429**, 259–283.

Clarke, J. F., Kassoy, D. R. & Riley, N. 1984 Shocks generated in a confined gas due to rapid heat addition at the boundary. I. Weak shock waves. II. Strong shock waves. *Proc. R. Soc. Lond.* A **393**, 309–351.

Clarke, J. F., Kassoy, D. R. & Riley, N. 1986 On the direct initiation of a plane detonation wave. *Proc. R. Soc. Lond.* A **408**, 129–148.

Dabora, E. K. 1972 Variable energy blast waves. *AIAA J.* **10**, 1384–1386.

Deshaies, B. & Clavin, P. 1979 Dynamic effects generated by a constant speed spherical flame. *J. Méc.* **18**, 213–223.

Freeman, R. A. 1968 Variable-energy blast waves. *Brit. J. Appl. Phys.* (*J. Phys.*) D **1**, 1697–1710.

Frendi, A. & Sibulkin, M. 1990 Dependences of minimum ignition energy on ignition parameters. *Combust. Sci. Tech.* **73**, 395–413.

Goldstine, H. H. & Neumann, J. 1955 Blast wave calculation. *Commun. Pure Appl. Maths* **8**, 327–354.

He, L. & Clavin, P. 1994 On the direct initiation of gaseous detonations by an energy source. *J. Fluid Mech.* **277**, 227–248.

Korobeinikov, V. P. 1971 Gas dynamics of explosions. *Annu. Rev. Fluid. Mech.* **3**, 317–346.

Korobeinikov, V. P. & Chushkin, P. I. 1966 Plane, cylindrical and spherical explosion in a gas with counter-pressure. In *Nonsteady Motions of Compressible Media with Blast Waves*, *Trudy Mat. Inst. V. A. Steklova*, vol. 87, pp. 4–33. Moscow: Nauka.

Kravchik, T. & Sher, E. 1994 Numerical modeling of spark ignition and flame initiation in a quiescent methane-air mixture. *Combust. Flame* **99**, 635–643.

Landau, L. D. 1945 On shock waves at large distances from the place of their origin. *Sov. J. Phys.* **9**, 496–500.

Landau, L. D. & Lifshitz, E. M. 1987 *Fluid Mechanics*, 2nd Edn. Chap. 89, pp. 333–335. Pergamon.

Maas, U. & Warnatz, J. 1988 Ignition processes in hydrogen-oxygen mixtures. *Combust. Flame* **74**, 53–69.

Meerson, B. 1989 On the dynamics of strong temperature disturbances in the upper atmosphere of the Earth. *Phys. Fluids* A **1**, 887–891.

Okhotsimskii, D. Ye. & Vlasova, Z. P. 1962 The behaviour of shock waves al large distances from the point of explosion. *Zh. Vych. Mat.* **2**, 107–124.

Rogers, M. H. 1958 Similarity flows behind strong shock waves. *Q. J. Mech. Appl. Maths* **11**, 411–422.

Sánchez, A. L., Jiménez-Alvarez, J. L. & Liñán, A. 2003 The coupling of motion and conductive heating of a gas by localized energy sources. *SIAM J. Appl. Maths* **63**, 937–961.

Sedov, L. I. 1946 Propagation of strong shock waves. *Prikl. Mat. Mekh.* **10**, 241–250.

Taylor, G. I. 1946 The air wave surrounding an expanding sphere. *Proc. R. Soc. Lond.* A **186**, 273–292.

Taylor, G. I. 1950 The formation of a blast wave by a very intense explosion. Part I. Theoretical discussion. Part II. The atomic explosion of 1945. *Proc. R. Soc. Lond.* A **201**, 159–186.

Thiele, M., Warnatz, J., Dreizler, A., Lindenmaier, S., Schiebl, R. & Maas, U. 2002 Spark ignited hydrogen/air mixtures: two-dimensional detailed modeling and laser based diagnostics. *Combust. Flame* **128**, 74–87

Thiele, M., Warnatz, J. & Maas, U. 2000 Geometrical study of spark ignition in two dimensions. *Combust. Theory Modell.* **4**, 413–434

Whitham, G. B. 1950 The propagation of spherical blast. *Proc. R. Soc. Lond.* A **203**, 571–581.

Zeldovich, Ya. B. & Kompaneetz, A. S. 1950 Towards a theory of heat conduction with thermal conductivity depending on the temperature. Collection of papers dedicated to 70th birthday of Academician A. F. Ioffe, *Izd. Akad. Nauk SSSR, Moscow*, pp. 61–71.